Published for SISSA by Springer

Received: *August 26, 2025*
Accepted: *September 17, 2025*
Published: *October 21, 2025*

Measurement of branching fractions and *CP* asymmetries in $\Lambda_b^0(\Xi_b^0) \to pK_S^0h^-$ decays

The LHCb collaboration

E-mail: chenzewen16@mails.ucas.ac.cn

Abstract: A study of Λ_b^0 and Ξ_b^0 baryon decays to the final states $pK_S^0\pi^-$ and $pK_S^0K^-$ is performed using pp collision data collected by the LHCb experiment, corresponding to an integrated luminosity of $9\,\text{fb}^{-1}$. The decays $\Lambda_b^0 \to pK_S^0K^-$ and $\Xi_b^0 \to pK_S^0K^-$ are observed for the first time, with significances reaching eight standard deviations. The branching fractions and integrated *CP* asymmetries are measured for the $\Lambda_b^0 \to pK_S^0\pi^-$, $\Lambda_b^0 \to pK_S^0K^-$, and $\Xi_b^0 \to pK_S^0K^-$ decays. For the decay $\Lambda_b^0 \to pK_S^0\pi^-$, the *CP* asymmetries are measured in different regions of the Dalitz plot. No evidence of *CP* violation is observed.

Keywords: B Physics, Branching fraction, CP Violation, Hadron-Hadron Scattering

ArXiv ePrint: 2508.17836

https://doi.org/10.1007/JHEP10(2025)169

JHEP10(2025)169

Contents

1 Introduction

In the Standard Model (SM) of particle physics, the combined charge conjugation (C) and parity (P) symmetry is not conserved in weak interactions (CP violation), as a consequence of an irreducible phase in the Cabibbo-Kobayashi-Maskawa (CKM) matrix [1]. Although all experimental measurements of CP violation in meson and baryon decays are compatible with the predictions of the CKM mechanism, the amount of CP violation in the SM is insufficient to account for the observed matter-antimatter imbalance in the Universe [2]. Extensive efforts have been dedicated to searches for CP violation in the sector of baryon decays [3–20], where only direct CP violation is expected. Additionally, the half-integer spin of baryons introduces more partial waves in baryon decays, making them more complex compared to meson decays. Recently, CP violation has been observed for the first time in baryon decays using the $\Lambda_b^0 \to pK^-\pi^+\pi^-$ decay [21],[1] and evidence for CP violation has been reported in the $\Lambda_b^0 \to \Lambda K^+K^-$ decay [22].

A large CP asymmetry is predicted in the $\Lambda_b^0 \to pK^*(892)^-$ decay, with values of $(19.7 \pm 1.4)\%$, $(31.1 \pm 2.8)\%$, and $(19.3 \pm 0.8)\%$ determined by the generalised factorisation approach (GFA) [23, 24], the QCD factorisation (QCDF) approach [25], and the light-front quark model (LFQM) under the GFA [26], respectively. Inspired by the recent measurement

[1]The inclusion of charge-conjugate processes is implied throughout the article if not specified otherwise.

JHEP10(2025)169

of *CP* asymmetries in the $\Lambda_b^0 \to p\pi^-$ and $\Lambda_b^0 \to pK^-$ decays [20], which are consistent with zero within 1% precision, two additional predictions find a much smaller *CP* asymmetry in the $\Lambda_b^0 \to pK^*(892)^-$ decay due to significant cancellation among the partial waves. These predictions are based on the perturbative QCD (pQCD) method [27] and the final-state rescattering mechanism [28], and correspond to a *CP* asymmetry of $(-5^{+10}_{-16})\%$ and $(2 \pm 4)\%$, respectively. The branching fraction of the $\Lambda_b^0 \to pK^*(892)^-$ decay is predicted to be approximately 10^{-6} by the GFA, the QCDF approach, and the LFQM approach, while the prediction incorporating the final-state rescattering mechanism suggests a significantly larger value of approximately 10^{-5}.

The $\Lambda_b^0 \to pK_S^0\pi^-$ decay was first observed by the LHCb experiment using proton-proton (pp) collision data corresponding to an integrated luminosity of $1\,\text{fb}^{-1}$, with a *CP* asymmetry of $(22 \pm 13 \pm 3)\%$ [3], where the first and second uncertainties are statistical and systematic, respectively. Since the $\Lambda_b^0 \to pK_S^0\pi^-$ decay proceeds through the quasi-two-body decay $\Lambda_b^0 \to pK^*(892)^-(\to K_S^0\pi^-)$, measurements of its *CP* asymmetry and branching fraction provide a stringent test of the aforementioned theoretical models, and offer new insights into the *CP* violation mechanism in baryon decays.

In this work, the branching fractions and the *CP*-violating observables of the charmless $\Lambda_b^0(\Xi_b^0) \to pK_S^0h^-$ decays, where h denotes either a pion or a kaon, are measured using pp collision data collected by the LHCb experiment during 2011–2012 (Run 1) and 2015–2018 (Run 2), at centre-of-mass energies of 7, 8 and 13 TeV, corresponding to an integrated luminosity of $9\,\text{fb}^{-1}$. The characteristics of the $\Lambda_b^0 \to pK_S^0K^-$, $\Xi_b^0 \to pK_S^0\pi^-$, and $\Xi_b^0 \to pK_S^0K^-$ decays are similar to those of the $\Lambda_b^0 \to pK_S^0\pi^-$ decay, where both tree and penguin amplitudes corresponding to the $b \to u\bar{u}q$ quark transition (with $q = d, s$) contribute at leading order. The interference between the tree and penguin amplitudes may result in *CP* violation. The *CP* asymmetries in different Dalitz-plot [29, 30] regions of the $\Lambda_b^0 \to pK_S^0\pi^-$ decay are also measured. To reduce the systematic uncertainties in these measurements, the $\Lambda_b^0 \to \Lambda_c^+(\to pK_S^0)\pi^-$ decay is used as a control channel. The $\Lambda_b^0 \to \Lambda_c^+(\to pK_S^0)K^-$ decay is employed as a control sample to calibrate the contribution from misidentified background in the $\Lambda_b^0 \to \Lambda_c^+(\to pK_S^0)\pi^-$ sample.

The paper is organised as follows. A brief description of the LHCb detector, trigger and simulation is presented in section 2. The event selection is presented in section 3. The measurements of branching fractions and *CP*-violating observables are presented in sections 4 and 5, respectively. Conclusions are given in section 6.

2 LHCb detector, trigger and simulation

The LHCb detector [31, 32] is a single-arm forward spectrometer covering the pseudorapidity range $2 < \eta < 5$, designed for the study of particles containing b or c quarks. The detector used for this work includes a high-precision tracking system consisting of a silicon-strip vertex detector surrounding the pp interaction region, a large-area silicon-strip detector located upstream of a dipole magnet with a bending power of about $4\,\text{T}\,\text{m}$, and three stations of silicon-strip detectors and straw drift tubes placed downstream of the magnet. The tracking system provides a measurement of the momentum, p, of charged particles with a relative uncertainty varying from 0.5% at low momentum to 1.0% at $200\,\text{GeV}/c$. The minimum

JHEP10(2025)169

distance of a track to a primary pp collision vertex (PV), the impact parameter (IP), is measured with a resolution of $(15 + 29/p_{\mathrm{T}})\,\mu\mathrm{m}$, where p_{T} is the component of the momentum transverse to the beam, in GeV/c. Different types of charged hadrons are distinguished using information from two ring-imaging Cherenkov detectors. Photons, electrons and hadrons are identified by a calorimeter system consisting of scintillating-pad and preshower detectors, an electromagnetic and a hadronic calorimeter. Muons are identified by a system composed of alternating layers of iron and multiwire proportional chambers.

The online event selection is performed by a trigger, which consists of a hardware stage, based on information from the calorimeter and muon systems, followed by a software stage, which applies a full event reconstruction. At the hardware trigger stage, events are required to have a muon with high p_{T} or a hadron, photon or electron with high transverse energy in the calorimeters. For hadrons, the transverse energy threshold is 3.5 GeV. The software trigger requires a two-, three- or four-track secondary vertex with a significant displacement from any primary pp interaction vertex. At least one charged particle must satisfy $p_{\mathrm{T}} > 1.6\,\mathrm{GeV}/c$ and be inconsistent with originating from a PV. A multivariate algorithm [33, 34] is used for the identification of secondary vertices consistent with the decay of a b hadron.

Simulation is required to model the effects of the detector acceptance, trigger, and the imposed selection requirements. In the simulation, pp collisions are generated using Pythia [35, 36] with a specific LHCb configuration [37]. Decays of unstable particles are described by EvtGen [38], in which final-state radiation is generated using Photos [39]. The interaction of the generated particles with the detector, and its response, are implemented using the Geant4 toolkit [40, 41] as described in ref. [42].

3 Event selection

The candidates for $\Lambda_b^0(\Xi_b^0) \to pK_{\mathrm{S}}^0 h^-$ decays are reconstructed by combining a K_{S}^0 candidate with two oppositely charged tracks identified as a proton and a pion or a kaon. The K_{S}^0 candidates are selected through the $K_{\mathrm{S}}^0 \to \pi^+\pi^-$ decay and are reconstructed in two categories. The first category consists of K_{S}^0 candidates reconstructed from two pion tracks with hits in both the vertex detector and the tracking detectors, referred to as the "long" K_{S}^0 candidates. The second category includes candidates reconstructed from two pion tracks with hits only in the tracking detectors, referred to as the "downstream" K_{S}^0 candidates. The final-state tracks (protons, pions, and kaons) are required to have a good track-fit quality and a high transverse momentum. The K_{S}^0 candidate must have a reconstructed decay vertex with a good vertex-fit quality, and a reconstructed mass within $\pm 20\,(30)\,\mathrm{MeV}/c^2$ of the known K_{S}^0 mass [43], for long (downstream) K_{S}^0 meson candidates. The $\Lambda_b^0(\Xi_b^0)$ reconstructed vertices are required to satisfy stringent vertex-fit quality criteria, while the reconstructed masses must be within $5420 < m(pK_{\mathrm{S}}^0 h^-) < 6200\,\mathrm{MeV}/c^2$. The K_{S}^0 decay vertex is selected to be downstream of the $\Lambda_b^0(\Xi_b^0)$ vertex by more than 15 mm along the beam.

Background from the $\Lambda \to p\pi^-$ decay, where the proton is misidentified as a pion, contributes to the K_{S}^0 mass spectrum. These candidates are rejected by applying a mass veto within $\pm 10\,\mathrm{MeV}/c^2$ of the known Λ mass [43] under the corresponding mass hypothesis. Background contributions from $B^0(B_s^0) \to K_{\mathrm{S}}^0 K^+ h^-$ decays, where a kaon is misidentified as a proton, contaminate the $\Lambda_b^0(\Xi_b^0)$ mass spectrum. These background sources are suppressed by

JHEP10(2025)169

applying a tight particle identification (PID) requirement on the proton for $\Lambda_b^0(\Xi_b^0)$ candidates whose reconstructed mass, calculated under the kaon mass hypothesis, lies within the $B(B_s^0)$ mass window $5245 < m(K_S^0 K^+ h^-) < 5402\,\text{MeV}/c^2$. Decays of the Λ_b^0 or Ξ_b^0 baryons through possible charm intermediate states, such as $\Xi_c^+ \to pK_S^0$, $D^- \to K_S^0\pi^-$, $D^- \to K_S^0 K^-$ and $D_s^- \to K_S^0 K^-$, are removed by applying mass vetoes within $\pm 30\,\text{MeV}/c^2$ of the known hadron masses [43]. For the higher-yield $\Lambda_c^+ \to pK_S^0$ decay, a wider veto region of $\pm 50\,\text{MeV}/c^2$ is used.

Boosted decision tree (BDT) classifiers [44, 45] are employed to further distinguish signal from background. Separate BDT classifiers are trained for the $pK_S^0\pi^-$ and $pK_S^0 K^-$ final states, for Run 1 and Run 2 periods, and for the two K_S^0 reconstruction categories. Simulated samples of $\Lambda_b^0 \to pK_S^0 h^-$ decays are used as signal training samples, while background proxies are obtained from data in the upper mass sideband region $5900 < m(pK_S^0 h^-) < 6200\,\text{MeV}/c^2$. The BDT classifiers utilise the kinematic and topological variables of the Λ_b^0 and K_S^0 hadrons and the PID variables of the proton and pion (or kaon) as inputs. The Λ_b^0 kinematics, track multiplicity, and PID distributions in simulated samples are corrected to match those observed in data. Two additional variables are included, both defined using tracks within a cone of radius $R = 1.5$ centred on the Λ_b^0 momentum direction, excluding those used to reconstruct the Λ_b^0 candidate, with $R = \sqrt{(\Delta\eta)^2 + (\Delta\phi)^2}$, where $\Delta\eta$ and $\Delta\phi$ denote the differences in pseudorapidity and azimuthal angle (in radians) between a given track and the Λ_b^0 candidate. The first variable is the track multiplicity within the cone, and the second is the transverse momentum asymmetry between the Λ_b^0 candidate and these tracks, defined as $(p_T(\Lambda_b^0) - \sum p_T(\text{track}))/(p_T(\Lambda_b^0) + \sum p_T(\text{track}))$. These two variables exploit additional information from tracks not associated with the Λ_b^0 candidate, enhancing the discrimination between signal and background. For the $\Lambda_b^0 \to pK_S^0\pi^-$ decay, the selection criterion on the BDT response is optimised to suppress the combinatorial background using a figure of merit (FoM), $S/\sqrt{S+B}$, where the S (B) denotes the estimated signal (background) yield in the Λ_b^0 signal region $5560 < m(pK_S^0 h^-) < 5680\,\text{MeV}/c^2$. The quantities S and B are obtained from a fit to data with a loose BDT requirement, and scaled by the BDT selection efficiencies, determined from simulation for signal and from sideband data for background. For the $\Lambda_b^0 \to pK_S^0 K^-$ decay, which is subject to sizeable contamination from the $pK_S^0\pi^-$ mode due to misidentification of the pion as a kaon, a simultaneous optimisation of the BDT response and the kaon PID requirement is performed. This optimisation suppresses both the combinatorial background and the misidentification contributions. It employs the Punzi FoM [46], $\epsilon/(a/2 + \sqrt{B})$, where ϵ denotes the signal efficiency in the Λ_b^0 signal region, $a = 5$ specifies the target significance of the signal component, and B is the sum of combinatorial and misidentified background yields in the signal region.

The $\Lambda_b^0 \to \Lambda_c^+(\to pK_S^0)h^-$ channels are selected using the same criteria as the $\Lambda_b^0 \to pK_S^0 h^-$ channels, except that the veto to the $\Lambda_c^+ \to pK_S^0$ decay is inverted, retaining only candidates within $\pm 30\,\text{MeV}/c^2$ of the known Λ_c^+ mass [43].

The fraction of events with multiple $\Lambda_b^0(\Xi_b^0)$ candidates is below 1%. In these events, one candidate is arbitrarily chosen.

JHEP10(2025)169

4 Measurement of branching fractions

The ratios of branching fractions between the $\Lambda_b^0(\Xi_b^0) \to pK_S^0h^-$ signal channels and the $\Lambda_b^0 \to \Lambda_c^+(\to pK_S^0)\pi^-$ control channel are defined and measured according to

$$\begin{aligned}\mathcal{R}(\Lambda_b^0 \to pK_S^0h^-) &\equiv \frac{\mathcal{B}(\Lambda_b^0 \to pK_S^0h^-)}{\mathcal{B}(\Lambda_b^0 \to \Lambda_c^+\pi^-)\mathcal{B}(\Lambda_c^+ \to pK_S^0)} \\ &= \frac{N(\Lambda_b^0 \to pK_S^0h^-)/\epsilon(\Lambda_b^0 \to pK_S^0h^-)}{N(\Lambda_b^0 \to \Lambda_c^+(\to pK_S^0)\pi^-)/\epsilon(\Lambda_b^0 \to \Lambda_c^+(\to pK_S^0)\pi^-)}, \end{aligned} \tag{4.1}$$

$$\begin{aligned}\mathcal{R}(\Xi_b^0 \to pK_S^0h^-) &\equiv \frac{\mathcal{B}(\Xi_b^0 \to pK_S^0h^-)}{\mathcal{B}(\Lambda_b^0 \to \Lambda_c^+\pi^-)\mathcal{B}(\Lambda_c^+ \to pK_S^0)} \\ &= \frac{N(\Xi_b^0 \to pK_S^0h^-)/\epsilon(\Xi_b^0 \to pK_S^0h^-)}{N(\Lambda_b^0 \to \Lambda_c^+(\to pK_S^0)\pi^-)/\epsilon(\Lambda_b^0 \to \Lambda_c^+(\to pK_S^0)\pi^-)} \times \frac{f_{\Lambda_b^0}}{f_{\Xi_b^0}}, \end{aligned} \tag{4.2}$$

where $\mathcal{B}$ denotes the branching fractions, N denotes the yields obtained from the fit to data, ϵ denotes the corresponding total efficiencies determined using simulation, and $f_{\Lambda_b^0(\Xi_b^0)}$ are the b-quark fragmentation fractions [47].

4.1 Mass fit

The $pK_S^0h^-$ mass distributions for the combined data of the Run 1 and Run 2 periods and the long and downstream K_S^0 categories (four data samples) after applying all selections are presented in figure 1. A mass constraint to the known K_S^0 mass is applied to the K_S^0 candidates to improve the resolution of the reconstructed $pK_S^0h^-$ mass. An extended unbinned maximum-likelihood fit is performed simultaneously to the invariant mass spectra of the four final states, $pK_S^0\pi^-$, $pK_S^0K^-$, $\Lambda_c^+(\to pK_S^0)\pi^-$, and $\Lambda_c^+(\to pK_S^0)K^-$ across the four data samples, resulting in a total of 16 samples, to extract the yields of $\Lambda_b^0(\Xi_b^0)$ signal components. The $\Lambda_b^0(\Xi_b^0)$ signal components are modelled using a modified Gaussian function with tails on both sides of the peak (double-sided Crystal Ball [48], DSCB). The peak position of the DSCB function, representing the mass of the Λ_b^0 or Ξ_b^0 baryon, is shared across all channels within the same data sample, with the mass difference between the Λ_b^0 and Ξ_b^0 baryons fixed to its known value [43]. The measured $\Lambda_b^0(\Xi_b^0)$ masses are found to be consistent across the four data samples. The width parameter of the DSCB function is parametrised as the square root of the quadratic sum of the value obtained from simulation and an additional common width term shared across all channels and data samples to account for the broader mass resolution observed in data. The tail parameters of the DSCB function are fixed to the values obtained from fits to simulated samples. The misidentified backgrounds from the $pK_S^0\pi^-$ and $pK_S^0K^-$ final states, due to the misidentification of a pion as a kaon or vice versa, are also modelled by DSCB functions, with their yields constrained based on the yields of the corresponding signal components and the efficiencies determined from simulation. For the $\Lambda_b^0 \to \Lambda_c^+(\to pK_S^0)\pi^-$ control channel, the $\Lambda_b^0 \to \Lambda_c^+(\to pK_S^0)K^-$ channel is used to constrain the yield of the misidentified background. The combinatorial background is modelled using an exponential function, with a slope parameter different for each channel and data sample, except for the $\Lambda_b^0 \to pK_S^0K^-$ sample, for which the slope is shared across the four data samples due to the small sample size. The partially reconstructed background from Λ_b^0 decays, with

JHEP10(2025)169

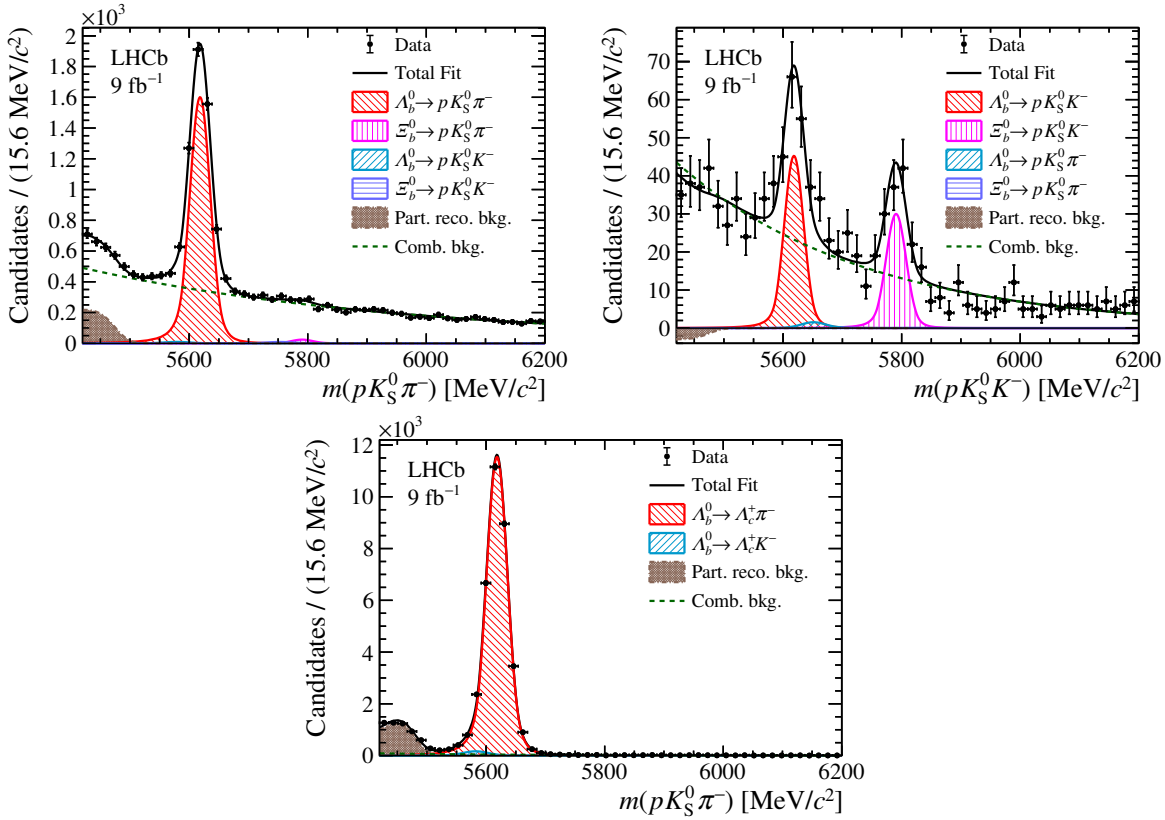

Figure 1. Mass distributions for the (top left) $\Lambda_b^0(\Xi_b^0) \to pK_S^0\pi^-$, (top right) $\Lambda_b^0(\Xi_b^0) \to pK_S^0K^-$, and (bottom) $\Lambda_b^0 \to \Lambda_c^+(\to pK_S^0)\pi^-$ decays, with the fit results also shown.

an additional π^0 meson that is not reconstructed, is modelled by an ARGUS function [49] convolved with a Gaussian resolution function. The parameter of the ARGUS function describing the mass cutoff is fixed to the known mass difference between the Λ_b^0 and π^0 hadrons [43]. The other shape parameters are free and shared across the four data samples of the same channel, except for the $\Lambda_b^0 \to pK_S^0K^-$ sample, for which the shape of the ARGUS function is fixed to that of the $\Lambda_b^0 \to pK_S^0\pi^-$ sample due to the small sample size. In the fit to the $\Lambda_b^0 \to pK_S^0K^-$ sample, the yield of the partially reconstructed background is found to be negative, but statistically consistent with zero.

The fit results for the $\Lambda_b^0(\Xi_b^0)$ signal yields, reported with statistical uncertainties only, are summarised in table 1. For the previously unobserved $\Lambda_b^0 \to pK_S^0K^-$, $\Xi_b^0 \to pK_S^0\pi^-$, and $\Xi_b^0 \to pK_S^0K^-$ decays, the corresponding significances, evaluated using Wilks' theorem [50] and taking into account systematic uncertainties as detailed later, are also reported. Systematic uncertainties are incorporated by evaluating the significance under alternative fit assumptions, with the smallest value quoted as the significance including systematic effects. Both the $\Lambda_b^0 \to pK_S^0K^-$ and the $\Xi_b^0 \to pK_S^0K^-$ decays are observed for the first time, with significances reaching 8 standard deviations (σ), indicating the discovery of these two decays, while no significant contribution of the $\Xi_b^0 \to pK_S^0\pi^-$ decay is observed. Consequently, the branching fractions of the $\Lambda_b^0 \to pK_S^0\pi^-$, $\Lambda_b^0 \to pK_S^0K^-$, and $\Xi_b^0 \to pK_S^0K^-$ decays are measured in this work, while an upper limit is set for the $\Xi_b^0 \to pK_S^0\pi^-$ decay.

JHEP10(2025)169

Decay	Yield	Significance
$\Lambda_b^0 \to pK_S^0\pi^-$	$4\,740 \pm 90$	—
$\Lambda_b^0 \to pK_S^0K^-$	127 ± 17	$8.1\,\sigma$
$\Xi_b^0 \to pK_S^0\pi^-$	70 ± 40	$1.0\,\sigma$
$\Xi_b^0 \to pK_S^0K^-$	88 ± 13	$8.0\,\sigma$
$\Lambda_b^0 \to \Lambda_c^+(\to pK_S^0)\pi^-$	$34\,680 \pm 200$	—

Table 1. Yields of the $\Lambda_b^0(\Xi_b^0)$ signal components presented with statistical uncertainties only. The corresponding significances, which include systematic uncertainties, are also provided. The significances of the previously observed $\Lambda_b^0 \to pK_S^0\pi^-$ and $\Lambda_b^0 \to \Lambda_c^+(\to pK_S^0)\pi^-$ decays are not evaluated.

4.2 Efficiencies

The total efficiency, including detector acceptance, reconstruction, trigger, and offline selection efficiencies, is estimated from simulation for each channel and data sample individually. To account for known discrepancies between simulation and data, several corrections are applied to the simulated samples. The tracking efficiency in simulation is corrected using large calibration samples from the $J/\psi \to \mu^+\mu^-$ decay [51]. Additionally, calibration samples from the $\Lambda \to p\pi^-$, $\Lambda_c^+ \to pK^-\pi^+$, and $D^{*+} \to D^0\pi^+$ decays are used to correct the mismodelling of PID information [52, 53] and trigger response [54] in simulation. The Λ_b^0 kinematics and track multiplicity in simulated Λ_b^0 decay samples are corrected by a weighting procedure [55]. The data and simulation samples of the $\Lambda_b^0 \to \Lambda_c^+(\to pK_S^0)\pi^-$ control channel are used as input to obtain the correction weights, which are subsequently applied to all simulated Λ_b^0 decay samples. As no control channel is available for Ξ_b^0 decays, the effect is incorporated as a systematic uncertainty for these decays. Finally, the kinematical phase-space distribution in simulation is corrected to match that in data. Since the Λ_b^0 baryon is unpolarised at LHCb [56, 57], the phase space of the $\Lambda_b^0 \to \Lambda_c^+(\to pK_S^0)\pi^-$ channel can be described using the Λ_c^+ helicity angle [58]. The simulated sample for the $\Lambda_b^0 \to \Lambda_c^+(\to pK_S^0)\pi^-$ decay is weighted to match the measured angular distribution [58]. For the $\Lambda_b^0(\Xi_b^0) \to pK_S^0h^-$ signal channels, the three-body phase space is described by the Dalitz-plot variables, $m^2(ph^-)$ and $m^2(K_S^0h^-)$, which are computed by constraining the reconstructed masses of the $\Lambda_b^0(\Xi_b^0)$ and K_S^0 candidates to their known values [43]. The background-subtracted Dalitz-plot distribution in data is obtained using the *sPlot* technique [59]. The simulated $\Lambda_b^0(\Xi_b^0) \to pK_S^0h^-$ samples are weighted to match the dynamics of the decay. The total efficiencies of the signal and control channels, estimated from the simulation samples after applying the same selection criteria as in data and incorporating all aforementioned corrections, are used to calculate the ratios of branching fractions.

4.3 Systematic uncertainties

Various sources of systematic uncertainty are taken into account for the measurement of the branching-fraction ratios. The dominant contribution arises from the efficiency estimation, including effects from the limited size of simulation samples and corrections applied to align the PID response and phase-space distribution in simulation with those observed in

JHEP10(2025)169

	Efficiency	Ξ_b^0 kinematics	Model	MisID bkg.	Ξ_b^0 bkg.	Total
$\mathcal{R}(\Lambda_b^0 \to pK_S^0\pi^-)$	1.4	—	0.3	0.1	—	1.5
$\mathcal{R}(\Lambda_b^0 \to pK_S^0K^-)$	6.4	—	3.6	1.3	5.7	9.3
$\mathcal{R}(\Xi_b^0 \to pK_S^0\pi^-) \times \frac{f_{\Xi_b^0}}{f_{\Lambda_b^0}}$	35.8	15.8	1.7	5.6	—	39.5
$\mathcal{R}(\Xi_b^0 \to pK_S^0K^-) \times \frac{f_{\Xi_b^0}}{f_{\Lambda_b^0}}$	9.1	5.9	4.8	1.0	4.6	12.7

Table 2. Relative systematic uncertainties in the ratios of branching fractions with respect to the $\Lambda_b^0 \to \Lambda_c^+(\to pK_S^0)\pi^-$ control channel, in percent. The total systematic uncertainties are obtained by summing the individual uncertainties in quadrature.

data. They are evaluated using pseudoexperiments and alternative calibration configurations, respectively. The largest systematic uncertainty in efficiency estimation stems from the correction of the Dalitz-plot distribution in the simulation of the $\Lambda_b^0(\Xi_b^0) \to pK_S^0h^-$ signal channels, as the distribution extracted from the background-subtracted data is subject to statistical fluctuations due to the limited signal yields. Furthermore, for Ξ_b^0 decays, the impact of differences in Ξ_b^0 kinematics between simulation and data is considered. The data and simulation samples are divided into regions of low and high Ξ_b^0 baryon p_T. The branching-fraction ratios are measured separately in each region and found to be in agreement within the statistical uncertainty. The difference between the combined result of these measurements and the baseline result is assigned as a systematic uncertainty.

Three additional sources of systematic uncertainty arise from the fit to the $pK_S^0h^-$ mass spectra. The first is due to the choice of fit models, assessed by employing alternative descriptions. The DSCB function is replaced with a Hypatia function [60], and the exponential function with a second-order Chebyshev polynomial. The model describing the partially reconstructed background is replaced with a shape extracted using kernel estimation [61] from simulated $\Lambda_b^0 \to pK^{*0}(\to K_S^0\pi^0)h^-$ and $\Lambda_b^0 \to \Sigma_c^+(\to \Lambda_c^+(\to pK_S^0)\pi^0)\pi^-$ samples, where the π^0 meson is not reconstructed, for the signal and control channels, respectively. The second source arises from the constraint on the yield of the misidentified background, estimated by varying the efficiency ratio of misidentification and signal components within its uncertainty. The third source is due to the potential partially reconstructed background from Ξ_b^0 decays in the $pK_S^0K^-$ mass spectra, which is not included in the baseline fit. The branching-fraction ratios of the $\Lambda_b^0(\Xi_b^0) \to pK_S^0K^-$ decays are measured by including this background, modelled using a shape extracted from a simulated $\Xi_b^0 \to pK^{*0}(\to K_S^0\pi^0)K^-$ sample with a missing π^0 meson, and with its yield fixed to that of the $\Xi_b^0 \to pK_S^0K^-$ signal component. The difference with respect to the baseline result is assigned as a systematic uncertainty. The fit procedure is validated using pseudoexperiments, and no bias is observed. However, the statistical uncertainties in the branching-fraction ratios of the $\Lambda_b^0(\Xi_b^0) \to pK_S^0\pi^-$ decays are found to be underestimated by 2.5 (3.8)% and are corrected accordingly. A summary of the systematic uncertainties is provided in table 2.

JHEP10(2025)169

	Result
$\mathcal{R}(\Lambda_b^0 \to pK_S^0\pi^-)$	$0.1363 \pm 0.0027 \pm 0.0020$
$\mathcal{R}(\Lambda_b^0 \to pK_S^0K^-)$	$0.0079 \pm 0.0010 \pm 0.0007$
$\mathcal{R}(\Xi_b^0 \to pK_S^0\pi^-) \times \frac{f_{\Xi_b^0}}{f_{\Lambda_b^0}}$	$< 0.0028\,(0.0031)$ at $90\,(95)\%$ CL
$\mathcal{R}(\Xi_b^0 \to pK_S^0K^-) \times \frac{f_{\Xi_b^0}}{f_{\Lambda_b^0}}$	$0.0041 \pm 0.0006 \pm 0.0005$

Table 3. Ratios of branching fractions with respect to the $\Lambda_b^0 \to \Lambda_c^+(\to pK_S^0)\pi^-$ control channel. The first uncertainty is statistical, and the second is systematic.

	Result $[\times 10^{-6}]$
$\mathcal{B}(\Lambda_b^0 \to pK_S^0\pi^-)$	$10.62 \pm 0.21 \pm 0.16 \pm 0.98$
$\mathcal{B}(\Lambda_b^0 \to pK_S^0K^-)$	$0.61 \pm 0.08 \pm 0.06 \pm 0.06$
$\mathcal{B}(\Xi_b^0 \to pK_S^0\pi^-)$	$< 2.8\,(3.2)$ at $90\,(95)\%$ CL
$\mathcal{B}(\Xi_b^0 \to pK_S^0K^-)$	$3.9 \pm 0.6 \pm 0.5 \pm 0.4 \pm 1.4$

Table 4. Branching fractions of the $\Lambda_b^0(\Xi_b^0) \to pK_S^0h^-$ decays. The first uncertainty is statistical, the second is systematic, and the third arises from the uncertainty in the branching fraction of the $\Lambda_b^0 \to \Lambda_c^+(\to pK_S^0)\pi^-$ control channel [43]. For Ξ_b^0 decays, a fourth uncertainty accounts for the b-quark fragmentation fractions [47].

4.4 Results

The measured ratios of branching fractions are listed in table 3. Since the significance of the $\Xi_b^0 \to pK_S^0\pi^-$ decay is only $1\,\sigma$, upper limits are set at 90% and 95% confidence levels (CL), by integrating the profile likelihood with a uniform Bayesian prior in the region of positive branching-fraction ratio. From the measurements of $\mathcal{B}(\Lambda_b^0 \to \Lambda_c^+\pi^-)$ and $\mathcal{B}(\Lambda_c^+ \to pK_S^0)$ [43], and the measurement of $f_{\Xi_b^0}/f_{\Lambda_b^0}$ [47], the absolute branching fractions of the $\Lambda_b^0(\Xi_b^0) \to pK_S^0h^-$ decays are extracted and summarised in table 4. The measured branching fraction of the $\Lambda_b^0 \to pK_S^0\pi^-$ decay agrees with, and supersedes, the previous measurement [3], with the statistical precision improved by a factor of nine.

5 Measurement of *CP*-violating observables

For the $\Lambda_b^0 \to pK_S^0\pi^-$, $\Lambda_b^0 \to pK_S^0K^-$, and $\Xi_b^0 \to pK_S^0K^-$ signal channels, all of which have significances exceeding five standard deviations, *CP*-violating observables are also measured. The *CP* asymmetry is defined as

$$\mathcal{A}^{CP}(\Lambda_b^0(\Xi_b^0) \to pK_S^0h^-) \equiv \frac{\Gamma(\Lambda_b^0(\Xi_b^0) \to pK_S^0h^-) - \Gamma(\overline{\Lambda}_b^0(\overline{\Xi}_b^0) \to \overline{p}K_S^0h^+)}{\Gamma(\Lambda_b^0(\Xi_b^0) \to pK_S^0h^-) + \Gamma(\overline{\Lambda}_b^0(\overline{\Xi}_b^0) \to \overline{p}K_S^0h^+)}, \tag{5.1}$$

where Γ represents the partial decay rate of the $\Lambda_b^0(\Xi_b^0) \to pK_S^0h^-$ decays or their charge-conjugate processes. The *CP* asymmetry is determined by correcting the raw asymmetry

JHEP10(2025)169

for several nuisance asymmetries,

$$\mathcal{A}^{CP} = \mathcal{A}^{\text{raw}} - \mathcal{A}^{\text{P}} - \mathcal{A}^{\text{D}} - \mathcal{A}^{\text{trigger}} - \mathcal{A}^{\text{PID}}, \tag{5.2}$$

where $\mathcal{A}^{\text{raw}} = (N - \overline{N})/(N + \overline{N})$ represents the raw asymmetry in the yields between the baryon and antibaryon modes, $\mathcal{A}^{\text{P}}$ accounts for the production asymmetry between $\Lambda_b^0(\Xi_b^0)$ and $\overline{\Lambda}_b^0(\overline{\Xi}_b^0)$ hadrons, $\mathcal{A}^{\text{D}}$ arises from differences in detection efficiency for final-state particles, excluding the effects of trigger and PID requirements, which are given by $\mathcal{A}^{\text{trigger}}$ and $\mathcal{A}^{\text{PID}}$, respectively. Since the CP asymmetry of the $\Lambda_b^0 \to \Lambda_c^+(\to pK_S^0)\pi^-$ decay is expected to be negligible in the SM, and its characteristics are similar to those of the $\Lambda_b^0(\Xi_b^0) \to pK_S^0 h^-$ signal channels, the difference in raw asymmetries between the signal and $\Lambda_b^0 \to \Lambda_c^+(\to pK_S^0)\pi^-$ control channels is measured to cancel most nuisance asymmetries. The $\mathcal{A}^{CP}$ of the signal channel is therefore extracted by subtracting the residual nuisance asymmetries,

$$\mathcal{A}^{CP} = \Delta\mathcal{A}^{\text{raw}} - \Delta\mathcal{A}^{\text{P}} - \Delta\mathcal{A}^{\text{D}} - \Delta\mathcal{A}^{\text{trigger}} - \Delta\mathcal{A}^{\text{PID}}, \tag{5.3}$$

where $\Delta\mathcal{A}^X$ denotes the difference in $\mathcal{A}^X$ between the signal and control channels.

5.1 Mass fit

The $pK_S^0 h^-$ mass distributions for the combined data of the four data samples, separated into baryon and antibaryon samples after applying all selection criteria, are shown in figure 2. An extended unbinned maximum-likelihood fit is performed simultaneously to all $pK_S^0 h^-$ mass spectra of the combined data, including the final states $pK_S^0\pi^-$, $pK_S^0 K^-$, $\Lambda_c^+(\to pK_S^0)\pi^-$, $\Lambda_c^+(\to pK_S^0)K^-$, and their charge-conjugate final states, resulting in a total of eight samples. The fit procedure follows that described in section 4, employing the same model for the corresponding components. The yields of each component are allowed to vary independently in the fit to the baryon and antibaryon samples. The difference in raw asymmetries between the signal and control channels is determined from this fit. The systematic uncertainties affecting the yields are evaluated using the same methods as described in section 4. The fit procedure is validated using pseudoexperiments, revealing a small bias in the $\Delta\mathcal{A}^{\text{raw}}(\Lambda_b^0 \to pK_S^0\pi^-)$ measurement, which is taken as a systematic uncertainty. Additionally, the statistical uncertainties in the $\Delta\mathcal{A}^{\text{raw}}(\Lambda_b^0 \to pK_S^0\pi^-)$ and $\Delta\mathcal{A}^{\text{raw}}(\Xi_b^0 \to pK_S^0 K^-)$ measurements are found to be underestimated by 2.5% and 2.2%, respectively, and corresponding corrections are applied. Systematic uncertainties in the fits are summarised in table 5.

5.2 Nuisance asymmetries

The Λ_b^0 production asymmetry in pp collisions at centre-of-mass energies of 7 and 8 TeV was measured by the LHCb collaboration as a function of p_{T} and rapidity (y) [62]. The $\mathcal{A}^{\text{P}}$ values for the $\Lambda_b^0 \to pK_S^0 h^-$ signal and $\Lambda_b^0 \to \Lambda_c^+(\to pK_S^0)\pi^-$ control channels are obtained by calculating the averaged Λ_b^0 production asymmetry, weighted by the two-dimensional p_{T} and y distributions in the corresponding background-subtracted data. Since no direct measurement of the Ξ_b^0 production asymmetry in pp collisions is available, the measurement of $\Delta\mathcal{A}^{\text{P}}$ between the $\Xi_b^- \to J/\psi\Xi^-$ and the $\Lambda_b^0 \to J/\psi\Lambda$ decays [47] is used to estimate the systematic uncertainty in the $\mathcal{A}^{CP}(\Xi_b^0 \to pK_S^0 K^-)$ measurement arising from residual production asymmetry by assuming isospin symmetry between the Ξ_b^0 and Ξ_b^- baryons. The

JHEP10(2025)169

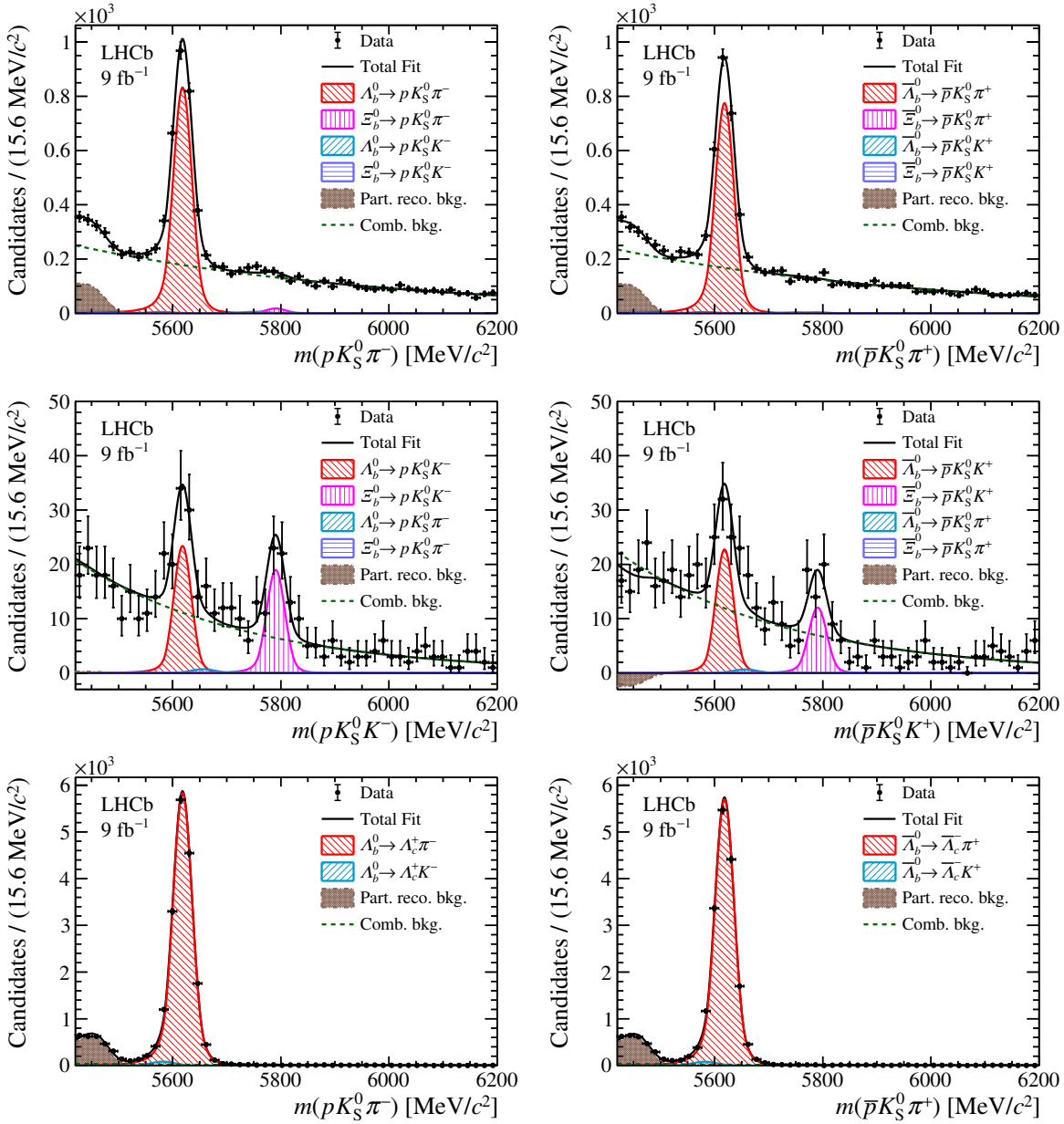

Figure 2. Mass distributions for the (top) $\Lambda_b^0(\Xi_b^0) \to p K_S^0 \pi^-$, (middle) $\Lambda_b^0(\Xi_b^0) \to p K_S^0 K^-$, and (bottom) $\Lambda_b^0 \to \Lambda_c^+(\to p K_S^0)\pi^-$ decays, shown separately for (left) baryon and (right) antibaryon samples. The fit results are also shown.

detection asymmetries for charged pions and kaons in momentum bins have been measured using $D^{*+} \to D^0(\to K^-\pi^+\pi^-\pi^+)\pi^+$, $D^+ \to K^-\pi^+\pi^+$, and $D^+ \to K_S^0\pi^+$ data [62]. For the detection asymmetry of protons, simulated samples of the $\Lambda_b^0 \to \Lambda_c^+(\to pK^-\pi^+)\mu^-\overline{\nu}_\mu$ decay are used [14]. The $\mathcal{A}^D$ values for pions, kaons and protons in the signal and control channels are obtained separately by calculating the averaged detection asymmetry weighted by the momentum distribution in the background-subtracted data. The asymmetry arising from different trigger responses to oppositely charged particles is measured using the

JHEP10(2025)169

	$\mathcal{A}^{CP}(\Lambda_b^0 \to pK_S^0\pi^-)$	$\mathcal{A}^{CP}(\Lambda_b^0 \to pK_S^0K^-)$	$\mathcal{A}^{CP}(\Xi_b^0 \to pK_S^0K^-)$
Model	< 0.1	0.4	1.0
MisID bkg.	< 0.1	0.2	1.2
Ξ_b^0 bkg.	—	7.5	5.6
Fit bias	0.1	—	—
$\mathcal{A}^{\mathrm{P}}(\Xi_b^0)$	—	—	6.3
$\mathcal{A}^{\mathrm{PID}}$	0.6	4.8	7.4
Residual asym.	0.7	1.6	0.6
Total	0.9	9.0	11.3

Table 5. Systematic uncertainties in the $\mathcal{A}^{CP}$ measurements for the $\Lambda_b^0 \to pK_S^0\pi^-$, $\Lambda_b^0 \to pK_S^0K^-$, and $\Xi_b^0 \to pK_S^0K^-$ decays, in percent. The total systematic uncertainties are obtained by summing the individual uncertainties in quadrature.

	Result [%]
$\mathcal{A}^{CP}$ $(\Lambda_b^0 \to pK_S^0\pi^-)$	$3.4 \pm 1.9 \pm 0.9$
$\mathcal{A}^{CP}$ $(\Lambda_b^0 \to pK_S^0K^-)$	$2 \pm 13 \pm 9$
$\mathcal{A}^{CP}$ $(\Xi_b^0 \to pK_S^0K^-)$	$22 \pm 15 \pm 11$

Table 6. *CP* asymmetries $\mathcal{A}^{CP}$ for the $\Lambda_b^0 \to pK_S^0\pi^-$, $\Lambda_b^0 \to pK_S^0K^-$, and $\Xi_b^0 \to pK_S^0K^-$ decays. The first uncertainty is statistical, and the second is systematic.

$\Lambda_b^0 \to \Lambda_c^+(\to pK^-\pi^+)\mu^-\overline{\nu}_\mu$ decay data, which includes pions, kaons and protons in the final state. The PID asymmetry is considered as a systematic uncertainty, and its effect is estimated using standard LHCb PID calibration tools [52, 53]. The systematic uncertainty in estimating the residual nuisance asymmetries is evaluated using pseudoexperiments, in which the measured asymmetries in bins of the relevant variables and the corresponding distributions in the background-subtracted data are randomly varied within their uncertainties. The resulting variation of the residual nuisance asymmetries is taken as the systematic uncertainty. The production and detection asymmetries reported in refs. [14, 62] were measured using *pp* collision data of the Run 1 period. These results are also applied to data of the Run 2 period in this work. The corresponding effect is evaluated and found to be negligible for the $\mathcal{A}^{CP}$ measurement at the current precision.

5.3 Results of integrated $\mathcal{A}^{CP}$

The $\mathcal{A}^{CP}$ values of the $\Lambda_b^0(\Xi_b^0) \to pK_S^0h^-$ signal channels are obtained by combining the measurements of $\Delta\mathcal{A}^{\mathrm{raw}}$ and residual nuisance asymmetries, as described in eq. (5.3), and are presented in table 6. The statistical precision of the *CP* asymmetry in the $\Lambda_b^0 \to pK_S^0\pi^-$ decay has improved by a factor of seven in comparison with the previous LHCb measurement [3]. No global *CP* violation is found in any of the three signal channels.

JHEP10(2025)169

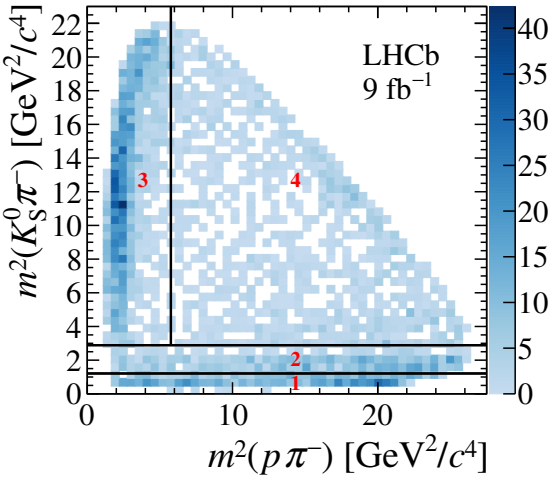

Figure 3. Dalitz plot of the $\Lambda_b^0 \to pK_S^0\pi^-$ decay, with background subtracted using the *sPlot* technique. The binning scheme for the $\mathcal{A}^{CP}$ measurements in phase-space regions is also shown.

	$m(p\pi^-)$	$m(K_S^0\pi^-)$	Yield	$\mathcal{A}^{CP}$ [%]
Bin 1	-	$< 1.1\,\text{GeV}/c^2$	821 ± 34	$-0.6 \pm 4.0 \pm 1.9$
Bin 2	-	$[1.1, 1.7]\,\text{GeV}/c^2$	870 ± 40	$12.4 \pm 4.2 \pm 1.8$
Bin 3	$\leq 2.4\,\text{GeV}/c^2$	$> 1.7\,\text{GeV}/c^2$	2200 ± 50	$0.5 \pm 2.4 \pm 1.1$
Bin 4	$> 2.4\,\text{GeV}/c^2$	$> 1.7\,\text{GeV}/c^2$	840 ± 50	$3.3 \pm 5.5 \pm 2.0$

Table 7. Measured $\mathcal{A}^{CP}$ results in different phase-space regions of the $\Lambda_b^0 \to pK_S^0\pi^-$ decay. The first uncertainty is statistical, and the second is systematic. The definitions for the four bins are also given. The corresponding Λ_b^0 signal yields in each bin are also reported, with their statistical uncertainties.

5.4 Results of $\mathcal{A}^{CP}(\Lambda_b^0 \to pK_S^0\pi^-)$ in Dalitz-plot regions

Given the substantial signal yield of $(4.74 \pm 0.09) \times 10^3$ in the $\Lambda_b^0 \to pK_S^0\pi^-$ decay, the *CP* asymmetry is also measured in different regions of the Dalitz plot. Figure 3 shows the Dalitz plot of the background-subtracted $\Lambda_b^0 \to pK_S^0\pi^-$ sample, divided into four bins according to the observed resonances: bin 1 corresponds to the $K^*(892)^-$ region, bin 2 to the region of the $K^*(1410)^-$, $K_0^*(1430)^-$, and $K_2^*(1430)^-$ resonances, bin 3 to the N^* region, and bin 4 to the nonresonant region. The same strategy used for the integrated $\mathcal{A}^{CP}$ measurement is applied to determine the $\mathcal{A}^{CP}$ values in these bins. For each bin, an extended unbinned maximum-likelihood fit is performed simultaneously to all $pK_S^0h^-$ mass spectra of the combined data, as in the integrated measurement. The only difference is that the total $\Lambda_b^0 \to pK_S^0\pi^-$ and $\overline{\Lambda}_b^0 \to \overline{p}K_S^0\pi^+$ samples are replaced by their respective subsamples within the given bin, while all other samples and the fit procedure remain unchanged. The $pK_S^0h^-$ mass distributions for the $\Lambda_b^0 \to pK_S^0\pi^-$ decay, divided into the four bins and further separated into baryon and antibaryon samples after applying all selection criteria, are shown in figure 4. The measured $\mathcal{A}^{CP}$ values, as well as the binning scheme, are summarised in table 7. All the $\mathcal{A}^{CP}$ values in

JHEP10(2025)169

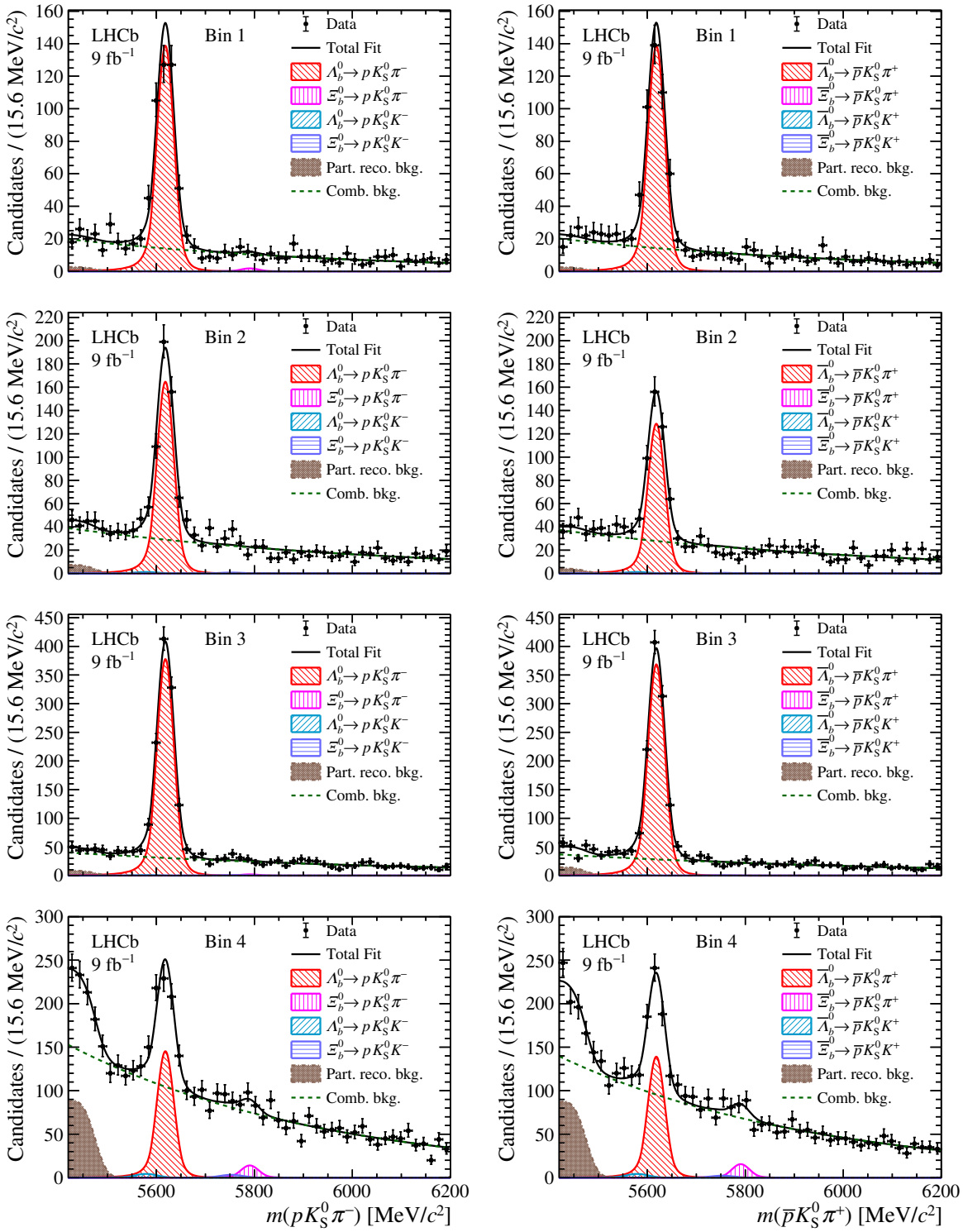

Figure 4. Mass distributions for the $\Lambda_b^0 \to pK_S^0\pi^-$ decay in Dalitz-plot bins 1 to 4 (from top to bottom), shown separately for (left) baryon and (right) antibaryon samples, with fit results.

JHEP10(2025)169

the four Dalitz-plot bins for the $\Lambda_b^0 \to pK_S^0\pi^-$ decay are consistent with zero, with the largest deviation observed in bin 2, corresponding to a significance of $2.7\,\sigma$ including systematic uncertainties. The $\mathcal{A}^{CP}$ value in the $K^*(892)^-$ dominated region is $(-0.6 \pm 4.0 \pm 1.9)\%$, where the first and second uncertainties are statistical and systematic, significantly smaller than the predicted value of 20% [23–26]. A possible explanation for this result is the cancellation of *CP* asymmetries among the partial waves in the $\Lambda_b^0 \to pK^*(892)^-$ decay [27, 28].

6 Conclusion

Using *pp* collision data collected by the LHCb experiment corresponding to an integrated luminosity of $9\,\text{fb}^{-1}$, the branching fractions for the $\Lambda_b^0 \to pK_S^0\pi^-$, $\Lambda_b^0 \to pK_S^0K^-$, and $\Xi_b^0 \to pK_S^0K^-$ decays are measured. The $\Lambda_b^0 \to pK_S^0K^-$ and $\Xi_b^0 \to pK_S^0K^-$ decays are observed for the first time, with significances reaching $8\,\sigma$. For the $\Xi_b^0 \to pK_S^0\pi^-$ decay, since the significance is less than $3\,\sigma$, upper limits are set. Integrated *CP* asymmetries are measured for all decays except for the $\Xi_b^0 \to pK_S^0\pi^-$ decay given the limited significance. Additionally, *CP* violation is studied in different Dalitz-plot regions of the $\Lambda_b^0 \to pK_S^0\pi^-$ decay. No *CP* violation is found in any of the signal decays with the current precision. The vanishing *CP* asymmetry observed for the $\Lambda_b^0 \to pK_S^0\pi^-$ decay in the $K^*(892)^-$ mass region, significantly smaller than the approximately 20% effect predicted by the GFA [23, 24], the QCDF approach [25], and the LFQM approach [26], is in agreement with the hypothesis of a cancellation mechanism among the contributing partial waves, as proposed in refs. [27, 28]. Further studies are needed to understand the mechanism of *CP* violation in baryon decays.

Acknowledgments

We express our gratitude to our colleagues in the CERN accelerator departments for the excellent performance of the LHC. We thank the technical and administrative staff at the LHCb institutes. We acknowledge support from CERN and from the national agencies: ARC (Australia); CAPES, CNPq, FAPERJ and FINEP (Brazil); MOST and NSFC (China); CNRS/IN2P3 (France); BMBF, DFG and MPG (Germany); INFN (Italy); NWO (Netherlands); MNiSW and NCN (Poland); MCID/IFA (Romania); MICIU and AEI (Spain); SNSF and SER (Switzerland); NASU (Ukraine); STFC (United Kingdom); DOE NP and NSF (U.S.A.). We acknowledge the computing resources that are provided by ARDC (Australia), CBPF (Brazil), CERN, IHEP and LZU (China), IN2P3 (France), KIT and DESY (Germany), INFN (Italy), SURF (Netherlands), Polish WLCG (Poland), IFIN-HH (Romania), PIC (Spain), CSCS (Switzerland), and GridPP (United Kingdom). We are indebted to the communities behind the multiple open-source software packages on which we depend. Individual groups or members have received support from Key Research Program of Frontier Sciences of CAS, CAS PIFI, CAS CCEPP, Fundamental Research Funds for the Central Universities, and Sci. & Tech. Program of Guangzhou (China); Minciencias (Colombia); EPLANET, Marie Skłodowska-Curie Actions, ERC and NextGenerationEU (European Union); A*MIDEX, ANR, IPhU and Labex P2IO, and Région Auvergne-Rhône-Alpes (France); Alexander-von-Humboldt Foundation (Germany); ICSC (Italy); Severo Ochoa and María de Maeztu Units of Excellence,

JHEP10(2025)169

GVA, XuntaGal, GENCAT, InTalent-Inditex and Prog. Atracción Talento CM (Spain); SRC (Sweden); the Leverhulme Trust, the Royal Society and UKRI (United Kingdom).

Data Availability Statement. Data associated to the plots in this publication as well as in supplementary materials are made available on the CERN document server at https://cds.cern.ch/record/2940941.

Code Availability Statement. This article has no associated code or the code will not be deposited.

JHEP10(2025)169

References

[1] M. Kobayashi and T. Maskawa, *CP violation in the renormalizable theory of weak interaction*, *Prog. Theor. Phys.* **49** (1973) 652 [INSPIRE].

[2] A. Riotto and M. Trodden, *Recent progress in baryogenesis*, *Ann. Rev. Nucl. Part. Sci.* **49** (1999) 35 [hep-ph/9901362] [INSPIRE].

[3] LHCb collaboration, *Searches for Λ_b^0 and Ξ_b^0 decays to $K_S^0 p\pi^-$ and $K_S^0 pK^-$ final states with first observation of the $\Lambda_b^0 \to K_S^0 p\pi^-$ decay*, *JHEP* **04** (2014) 087 [arXiv:1402.0770] [INSPIRE].

[4] LHCb collaboration, *Observation of the $\Lambda_b^0 \to J/\psi p\pi^-$ decay*, *JHEP* **07** (2014) 103 [arXiv:1406.0755] [INSPIRE].

[5] LHCb collaboration, *Observation of the $\Lambda_b^0 \to \Lambda\phi$ decay*, *Phys. Lett. B* **759** (2016) 282 [arXiv:1603.02870] [INSPIRE].

[6] LHCb collaboration, *Observations of $\Lambda_b^0 \to \Lambda K^+\pi^-$ and $\Lambda_b^0 \to \Lambda K^+K^-$ decays and searches for other Λ_b^0 and Ξ_b^0 decays to $\Lambda h^+h'^-$ final states*, *JHEP* **05** (2016) 081 [arXiv:1603.00413] [INSPIRE].

[7] LHCb collaboration, *Measurement of matter-antimatter differences in beauty baryon decays*, *Nature Phys.* **13** (2017) 391 [arXiv:1609.05216] [INSPIRE].

[8] LHCb collaboration, *Search for CP violation and observation of P violation in $\Lambda_b^0 \to p\pi^-\pi^+\pi^-$ decays*, *Phys. Rev. D* **102** (2020) 051101 [arXiv:1912.10741] [INSPIRE].

[9] LHCb collaboration, *Observation of the decay $\Lambda_b^0 \to pK^-\mu^+\mu^-$ and a search for CP violation*, *JHEP* **06** (2017) 108 [arXiv:1703.00256] [INSPIRE].

[10] LHCb collaboration, *A measurement of the CP asymmetry difference in $\Lambda_c^+ \to pK^-K^+$ and $p\pi^-\pi^+$ decays*, *JHEP* **03** (2018) 182 [arXiv:1712.07051] [INSPIRE].

[11] LHCb collaboration, *Search for CP violation using triple product asymmetries in $\Lambda_b^0 \to pK^-\pi^+\pi^-$, $\Lambda_b^0 \to pK^-K^+K^-$ and $\Xi_b^0 \to pK^-K^-\pi^+$ decays*, *JHEP* **08** (2018) 039 [arXiv:1805.03941] [INSPIRE].

[12] CDF collaboration, *Measurements of direct CP violating asymmetries in charmless decays of strange bottom mesons and bottom baryons*, *Phys. Rev. Lett.* **106** (2011) 181802 [arXiv:1103.5762] [INSPIRE].

[13] CDF collaboration, *Measurements of direct CP-violating asymmetries in charmless decays of bottom baryons*, *Phys. Rev. Lett.* **113** (2014) 242001 [arXiv:1403.5586] [INSPIRE].

[14] LHCb collaboration, *Search for CP violation in $\Lambda_b^0 \to pK^-$ and $\Lambda_b^0 \to p\pi^-$ decays*, *Phys. Lett. B* **787** (2018) 124 [arXiv:1807.06544] [INSPIRE].

[15] LHCb collaboration, *Measurements of CP asymmetries in charmless four-body Λ_b^0 and Ξ_b^0 decays*, *Eur. Phys. J. C* **79** (2019) 745 [arXiv:1903.06792] [INSPIRE].

[16] LHCb collaboration, *Search for CP violation in $\Xi_c^+ \to pK^-\pi^+$ decays using model-independent techniques*, *Eur. Phys. J. C* **80** (2020) 986 [arXiv:2006.03145] [INSPIRE].

[17] LHCb collaboration, *Search for CP violation in $\Xi_b^- \to pK^-K^-$ decays*, *Phys. Rev. D* **104** (2021) 052010 [arXiv:2104.15074] [INSPIRE].

[18] LHCb collaboration, *Observation of the suppressed $\Lambda_b^0 \to DpK^-$ decay with $D \to K^+\pi^-$ and measurement of its CP asymmetry*, *Phys. Rev. D* **104** (2021) 112008 [arXiv:2109.02621] [INSPIRE].

[19] LHCb collaboration, *Measurement of the photon polarization in $\Lambda_b^0 \to \Lambda\,\gamma$ decays*, *Phys. Rev. D* **105** (2022) L051104 [arXiv:2111.10194] [INSPIRE].

[20] LHCb collaboration, *Measurement of CP asymmetries in $\Lambda_b^0 \to ph^-$ decays*, *Phys. Rev. D* **111** (2025) 092004 [arXiv:2412.13958] [INSPIRE].

[21] LHCb collaboration, *Observation of charge–parity symmetry breaking in baryon decays*, *Nature* **643** (2025) 1223 [arXiv:2503.16954] [INSPIRE].

[22] LHCb collaboration, *Study of Λ_b^0 and Ξ_b^0 decays to $\Lambda h^+h'^-$ and evidence for CP violation in $\Lambda_b^0 \to \Lambda K^+K^-$*, *Phys. Rev. Lett.* **134** (2025) 101802 [arXiv:2411.15441] [INSPIRE].

[23] Y.K. Hsiao and C.Q. Geng, *Direct CP violation in Λ_b decays*, *Phys. Rev. D* **91** (2015) 116007 [arXiv:1412.1899] [INSPIRE].

[24] Y.K. Hsiao, Y. Yao and C.Q. Geng, *Charmless two-body anti-triplet b-baryon decays*, *Phys. Rev. D* **95** (2017) 093001 [arXiv:1702.05263] [INSPIRE].

[25] J. Zhu, Z.-T. Wei and H.-W. Ke, *Semileptonic and nonleptonic weak decays of Λ_b^0*, *Phys. Rev. D* **99** (2019) 054020 [arXiv:1803.01297] [INSPIRE].

[26] C.Q. Geng, C.-W. Liu and T.-H. Tsai, *Non-leptonic two-body decays of Λ_b^0 in light-front quark model*, *Phys. Lett. B* **815** (2021) 136125 [arXiv:2102.01552] [INSPIRE].

[27] J.-J. Han et al., *Establishing CP violation in b-baryon decays*, *Phys. Rev. Lett.* **134** (2025) 221801 [arXiv:2409.02821] [INSPIRE].

[28] Z.-D. Duan et al., *Final-state rescattering mechanism in bottom-baryon decays*, *JHEP* **09** (2025) 160 [arXiv:2412.20458] [INSPIRE].

[29] R.H. Dalitz, *On the analysis of tau-meson data and the nature of the tau-meson*, *Phil. Mag. Ser. 7* **44** (1953) 1068 [INSPIRE].

[30] E. Fabri, *A study of tau-meson decay*, *Nuovo Cim.* **11** (1954) 479 [INSPIRE].

[31] LHCb collaboration, *The LHCb detector at the LHC*, 2008 *JINST* **3** S08005 [INSPIRE].

[32] LHCb collaboration, *LHCb detector performance*, *Int. J. Mod. Phys. A* **30** (2015) 1530022 [arXiv:1412.6352] [INSPIRE].

[33] V.V. Gligorov and M. Williams, *Efficient, reliable and fast high-level triggering using a bonsai boosted decision tree*, 2013 *JINST* **8** P02013 [arXiv:1210.6861] [INSPIRE].

JHEP10(2025)169

[34] T. Likhomanenko et al., *LHCb topological trigger reoptimization*, *J. Phys. Conf. Ser.* **664** (2015) 082025 [arXiv:1510.00572] [INSPIRE].

[35] T. Sjöstrand, S. Mrenna and P.Z. Skands, *A brief introduction to PYTHIA 8.1*, *Comput. Phys. Commun.* **178** (2008) 852 [arXiv:0710.3820] [INSPIRE].

[36] T. Sjöstrand, S. Mrenna and P.Z. Skands, *PYTHIA 6.4 physics and manual*, *JHEP* **05** (2006) 026 [hep-ph/0603175] [INSPIRE].

[37] I. Belyaev et al., *Handling of the generation of primary events in Gauss, the LHCb simulation framework*, *J. Phys. Conf. Ser.* **331** (2011) 032047 [INSPIRE].

[38] D.J. Lange, *The EvtGen particle decay simulation package*, *Nucl. Instrum. Meth. A* **462** (2001) 152 [INSPIRE].

[39] N. Davidson, T. Przedzinski and Z. Was, *PHOTOS interface in C++: technical and physics documentation*, *Comput. Phys. Commun.* **199** (2016) 86 [arXiv:1011.0937] [INSPIRE].

[40] J. Allison et al., *GEANT4 developments and applications*, *IEEE Trans. Nucl. Sci.* **53** (2006) 270 [INSPIRE].

[41] GEANT4 collaboration, *GEANT4 — a simulation toolkit*, *Nucl. Instrum. Meth. A* **506** (2003) 250 [INSPIRE].

[42] M. Clemencic et al., *The LHCb simulation application, Gauss: design, evolution and experience*, *J. Phys. Conf. Ser.* **331** (2011) 032023 [INSPIRE].

[43] Particle Data Group collaboration, *Review of particle physics*, *Phys. Rev. D* **110** (2024) 030001 [INSPIRE].

[44] L. Breiman, J. Friedman, R.A. Olshen and C.J. Stone, *Classification and regression trees*, Chapman and Hall/CRC, U.S.A. (2017) [DOI:10.1201/9781315139470] [INSPIRE].

[45] Y. Freund and R.E. Schapire, *A decision-theoretic generalization of on-line learning and an application to boosting*, *J. Comput. Syst. Sci.* **55** (1997) 119 [INSPIRE].

[46] G. Punzi, *Sensitivity of searches for new signals and its optimization*, *eConf C* **030908** (2003) MODT002 [physics/0308063] [INSPIRE].

[47] LHCb collaboration, *Measurement of the mass and production rate of Ξ_b^- baryons*, *Phys. Rev. D* **99** (2019) 052006 [arXiv:1901.07075] [INSPIRE].

[48] T. Skwarnicki, *A study of the radiative CASCADE transitions between the Upsilon-Prime and Upsilon resonances*, Ph.D. thesis, INP, Cracow, Poland (1986) [INSPIRE].

[49] ARGUS collaboration, *Search for hadronic $b \to u$ decays*, *Phys. Lett. B* **241** (1990) 278 [INSPIRE].

[50] S.S. Wilks, *The large-sample distribution of the likelihood ratio for testing composite hypotheses*, *Annals Math. Statist.* **9** (1938) 60 [INSPIRE].

[51] LHCb collaboration, *Measurement of the track reconstruction efficiency at LHCb*, 2015 *JINST* **10** P02007 [arXiv:1408.1251] [INSPIRE].

[52] L. Anderlini et al., *The PIDCalib package*, LHCb-PUB-2016-021, CERN, Geneva, Switzerland (2016) [INSPIRE].

[53] R. Aaij et al., *Selection and processing of calibration samples to measure the particle identification performance of the LHCb experiment in run 2*, *EPJ Tech. Instrum.* **6** (2019) 1 [arXiv:1803.00824] [INSPIRE].

JHEP10(2025)169

[54] R. Aaij et al., *The LHCb trigger and its performance in 2011*, 2013 *JINST* **8** P04022 [arXiv:1211.3055] [INSPIRE].

[55] A. Rogozhnikov, *Reweighting with boosted decision trees*, *J. Phys. Conf. Ser.* **762** (2016) 012036 [arXiv:1608.05806] [INSPIRE].

[56] LHCb collaboration, *Measurements of the $\Lambda_b^0 \to J/\psi\Lambda$ decay amplitudes and the Λ_b^0 polarisation in pp collisions at $\sqrt{s} = 7$ TeV*, *Phys. Lett. B* **724** (2013) 27 [arXiv:1302.5578] [INSPIRE].

[57] LHCb collaboration, *Measurement of the $\Lambda_b^0 \to J/\psi\Lambda$ angular distribution and the Λ_b^0 polarisation in pp collisions*, *JHEP* **06** (2020) 110 [arXiv:2004.10563] [INSPIRE].

[58] LHCb collaboration, *Measurement of Λ_b^0, Λ_c^+ and Λ decay parameters using $\Lambda_b^0 \to \Lambda_c^+ h^-$ decays*, *Phys. Rev. Lett.* **133** (2024) 261804 [arXiv:2409.02759] [INSPIRE].

[59] M. Pivk and F.R. Le Diberder, *SPlot: a statistical tool to unfold data distributions*, *Nucl. Instrum. Meth. A* **555** (2005) 356 [physics/0402083] [INSPIRE].

[60] D. Martínez Santos and F. Dupertuis, *Mass distributions marginalized over per-event errors*, *Nucl. Instrum. Meth. A* **764** (2014) 150 [arXiv:1312.5000] [INSPIRE].

[61] K.S. Cranmer, *Kernel estimation in high-energy physics*, *Comput. Phys. Commun.* **136** (2001) 198 [hep-ex/0011057] [INSPIRE].

[62] LHCb collaboration, *Measurement of B^0, B_s^0, B^+ and Λ_b^0 production asymmetries in 7 and 8 TeV proton-proton collisions*, *Phys. Lett. B* **774** (2017) 139 [arXiv:1703.08464] [INSPIRE].

JHEP10(2025)169

The LHCb collaboration

R. Aaij[38], A.S.W. Abdelmotteleb[57], C. Abellan Beteta[51], F. Abudinén[57], T. Ackernley[61], A. A. Adefisoye[69], B. Adeva[47], M. Adinolfi[55], P. Adlarson[84], C. Agapopoulou[14], C.A. Aidala[86], Z. Ajaltouni[11], S. Akar[11], K. Akiba[38], P. Albicocco[28], J. Albrecht[19,g], F. Alessio[49], Z. Aliouche[63], P. Alvarez Cartelle[56], R. Amalric[16], S. Amato[3], J.L. Amey[55], Y. Amhis[14], L. An[6], L. Anderlini[27], M. Andersson[51], P. Andreola[51], M. Andreotti[26], S. Andres Estrada[83], A. Anelli[31,p,49], D. Ao[7], F. Archilli[37,w], Z Areg[69], M. Argenton[26], S. Arguedas Cuendis[9,49], A. Artamonov[44], M. Artuso[69], E. Aslanides[13], R. Ataíde Da Silva[50], M. Atzeni[65], B. Audurier[12], J. A. Authier[15], D. Bacher[64], I. Bachiller Perea[50], S. Bachmann[22], M. Bachmayer[50], J.J. Back[57], P. Baladron Rodriguez[47], V. Balagura[15], A. Balboni[26], W. Baldini[26], L. Balzani[19], H. Bao[7], J. Baptista de Souza Leite[61], C. Barbero Pretel[47,12], M. Barbetti[27], I. R. Barbosa[70], R.J. Barlow[63], M. Barnyakov[25], S. Barsuk[14], W. Barter[59], J. Bartz[69], S. Bashir[40], B. Batsukh[5], P. B. Battista[14], A. Bay[50], A. Beck[65], M. Becker[19], F. Bedeschi[35], I.B. Bediaga[2], N. A. Behling[19], S. Belin[47], K. Belous[44], I. Belov[29], I. Belyaev[36], G. Benane[13], G. Bencivenni[28], E. Ben-Haim[16], A. Berezhnoy[44], R. Bernet[51], S. Bernet Andres[46], A. Bertolin[33], C. Betancourt[51], F. Betti[59], J. Bex[56], Ia. Bezshyiko[51], O. Bezshyyko[85], J. Bhom[41], M.S. Bieker[18], N.V. Biesuz[26], P. Billoir[16], A. Biolchini[38], M. Birch[62], F.C.R. Bishop[10], A. Bitadze[63], A. Bizzeti[27,q], T. Blake[57,c], F. Blanc[50], J.E. Blank[19], S. Blusk[69], V. Bocharnikov[44], J.A. Boelhauve[19], O. Boente Garcia[15], T. Boettcher[68], A. Bohare[59], A. Boldyrev[44], C.S. Bolognani[81], R. Bolzonella[26,m], R. B. Bonacci[1], N. Bondar[44,49], A. Bordelius[49], F. Borgato[33,49], S. Borghi[63], M. Borsato[31,p], J.T. Borsuk[82], E. Bottalico[61], S.A. Bouchiba[50], M. Bovill[64], T.J.V. Bowcock[61], A. Boyer[49], C. Bozzi[26], J. D. Brandenburg[87], A. Brea Rodriguez[50], N. Breer[19], J. Brodzicka[41], A. Brossa Gonzalo[47,†], J. Brown[61], D. Brundu[32], E. Buchanan[59], L. Buonincontri[33,r], M. Burgos Marcos[81], A.T. Burke[63], C. Burr[49], J.S. Butter[56], J. Buytaert[49], W. Byczynski[49], S. Cadeddu[32], H. Cai[74], Y. Cai[5], A. Caillet[16], R. Calabrese[26,m], S. Calderon Ramirez[9], L. Calefice[45], S. Cali[28], M. Calvi[31,p], M. Calvo Gomez[46], P. Camargo Magalhaes[2,a], J. I. Cambon Bouzas[47], P. Campana[28], D.H. Campora Perez[81], A.F. Campoverde Quezada[7], S. Capelli[31], L. Capriotti[26], R. Caravaca-Mora[9], A. Carbone[25,k], L. Carcedo Salgado[47], R. Cardinale[29,n], A. Cardini[32], P. Carniti[31], L. Carus[22], A. Casais Vidal[65], R. Caspary[22], G. Casse[61], M. Cattaneo[49], G. Cavallero[26], V. Cavallini[26,m], S. Celani[22], S. Cesare[30,o], A.J. Chadwick[61], I. Chahrour[86], H. Chang[4,d], M. Charles[16], Ph. Charpentier[49], E. Chatzianagnostou[38], R. Cheaib[78], M. Chefdeville[10], C. Chen[56], J. Chen[50], S. Chen[5], Z. Chen[7], M. Cherif[12], A. Chernov[41], S. Chernyshenko[53], X. Chiotopoulos[81], V. Chobanova[83], M. Chrzaszcz[41], A. Chubykin[44], V. Chulikov[28,36], P. Ciambrone[28], X. Cid Vidal[47], G. Ciezarek[49], P. Cifra[38], P.E.L. Clarke[59], M. Clemencic[49], H.V. Cliff[56], J. Closier[49], C. Cocha Toapaxi[22], V. Coco[49], J. Cogan[13], E. Cogneras[11], L. Cojocariu[43], S. Collaviti[50], P. Collins[49], T. Colombo[49], M. Colonna[19], A. Comerma-Montells[45], L. Congedo[24], J. Connaughton[57], A. Contu[32], N. Cooke[60], C. Coronel[66], I. Corredoira[12], A. Correia[16], G. Corti[49], J. Cottee Meldrum[55], B. Couturier[49], D.C. Craik[51], M. Cruz Torres[2,h], E. Curras Rivera[50], R. Currie[59],

JHEP10(2025)169

C.L. Da Silva[68], S. Dadabaev[44], L. Dai[71], X. Dai[4], E. Dall'Occo[49], J. Dalseno[83], C. D'Ambrosio[62], J. Daniel[11], P. d'Argent[24], G. Darze[3], A. Davidson[57], J.E. Davies[63], O. De Aguiar Francisco[63], C. De Angelis[32,l], F. De Benedetti[49], J. de Boer[38], K. De Bruyn[80], S. De Capua[63], M. De Cian[63], U. De Freitas Carneiro Da Graca[2,b], E. De Lucia[28], J.M. De Miranda[2], L. De Paula[3], M. De Serio[24,i], P. De Simone[28], F. De Vellis[19], J.A. de Vries[81], F. Debernardis[24], D. Decamp[10], S. Dekkers[1], L. Del Buono[16], B. Delaney[65], H.-P. Dembinski[19], J. Deng[8], V. Denysenko[51], O. Deschamps[11], F. Dettori[32,l], B. Dey[78], P. Di Nezza[28], I. Diachkov[44], S. Didenko[44], S. Ding[69], Y. Ding[50], L. Dittmann[22], V. Dobishuk[53], A. D. Docheva[60], A. Doheny[57], C. Dong[4,d], A.M. Donohoe[23], F. Dordei[32], A.C. dos Reis[2], A. D. Dowling[69], L. Dreyfus[13], W. Duan[72], P. Duda[82], M.W. Dudek[41], L. Dufour[49], V. Duk[34], P. Durante[49], M. M. Duras[82], J.M. Durham[68], O. D. Durmus[78], A. Dziurda[41], A. Dzyuba[44], S. Easo[58], E. Eckstein[18], U. Egede[1], A. Egorychev[44], V. Egorychev[44], S. Eisenhardt[59], E. Ejopu[63], L. Eklund[84], M. Elashri[66], J. Ellbracht[19], S. Ely[62], A. Ene[43], J. Eschle[69], S. Esen[22], T. Evans[38], F. Fabiano[32], S. Faghih[66], L.N. Falcao[2], B. Fang[7], R. Fantechi[35], L. Fantini[34,s], M. Faria[50], K. Farmer[59], D. Fazzini[31,p], L. Felkowski[82], M. Feng[5,7], M. Feo[19], A. Fernandez Casani[48], M. Fernandez Gomez[47], A.D. Fernez[67], F. Ferrari[25,k], F. Ferreira Rodrigues[3], M. Ferrillo[51], M. Ferro-Luzzi[49], S. Filippov[44], R.A. Fini[24], M. Fiorini[26,m], M. Firlej[40], K.L. Fischer[64], D.S. Fitzgerald[86], C. Fitzpatrick[63], T. Fiutowski[40], F. Fleuret[15], A. Fomin[52], M. Fontana[25], L. F. Foreman[63], R. Forty[49], D. Foulds-Holt[59], V. Franco Lima[3], M. Franco Sevilla[67], M. Frank[49], E. Franzoso[26,m], G. Frau[63], C. Frei[49], D.A. Friday[63], J. Fu[7], Q. Führing[19,g,56], T. Fulghesu[13], G. Galati[24], M.D. Galati[38], A. Gallas Torreira[47], D. Galli[25,k], S. Gambetta[59], M. Gandelman[3], P. Gandini[30], B. Ganie[63], H. Gao[7], R. Gao[64], T.Q. Gao[56], Y. Gao[8], Y. Gao[6], Y. Gao[8], L.M. Garcia Martin[50], P. Garcia Moreno[45], J. García Pardiñas[65], P. Gardner[67], K. G. Garg[8], L. Garrido[45], C. Gaspar[49], A. Gavrikov[33], L.L. Gerken[19], E. Gersabeck[20], M. Gersabeck[20], T. Gershon[57], S. Ghizzo[29,n], Z. Ghorbanimoghaddam[55], L. Giambastiani[33,r], F. I. Giasemis[16,f], V. Gibson[56], H.K. Giemza[42], A.L. Gilman[64], M. Giovannetti[28], A. Gioventù[45], L. Girardey[63,58], M.A. Giza[41], F.C. Glaser[14,22], V.V. Gligorov[16], C. Göbel[70], L. Golinka-Bezshyyko[85], E. Golobardes[46], D. Golubkov[44], A. Golutvin[62,49], S. Gomez Fernandez[45], W. Gomulka[40], I. Gonçales Vaz[49], F. Goncalves Abrantes[64], M. Goncerz[41], G. Gong[4,d], J. A. Gooding[19], I.V. Gorelov[44], C. Gotti[31], E. Govorkova[65], J.P. Grabowski[18], L.A. Granado Cardoso[49], E. Graugés[45], E. Graverini[50,u], L. Grazette[57], G. Graziani[27], A. T. Grecu[43], L.M. Greeven[38], N.A. Grieser[66], L. Grillo[60], S. Gromov[44], C. Gu[15], M. Guarise[26], L. Guerry[11], V. Guliaeva[44], P. A. Günther[22], A.-K. Guseinov[50], E. Gushchin[44], Y. Guz[6,49], T. Gys[49], K. Habermann[18], T. Hadavizadeh[1], C. Hadjivasiliou[67], G. Haefeli[50], C. Haen[49], S. Haken[56], G. Hallett[57], P.M. Hamilton[67], J. Hammerich[61], Q. Han[33], X. Han[22,49], S. Hansmann-Menzemer[22], L. Hao[7], N. Harnew[64], T. H. Harris[1], M. Hartmann[14], S. Hashmi[40], J. He[7,e], A. Hedes[63], F. Hemmer[49], C. Henderson[66], R. Henderson[14], R.D.L. Henderson[1], A.M. Hennequin[49], K. Hennessy[61], L. Henry[50], J. Herd[62], P. Herrero Gascon[22], J. Heuel[17], A. Hicheur[3], G. Hijano Mendizabal[51], J. Horswill[63], R. Hou[8], Y. Hou[11], D.

JHEP10(2025)169

C. Houston[60], N. Howarth[61], J. Hu[72], W. Hu[7], X. Hu[4,d], W. Hulsbergen[38], R.J. Hunter[57], M. Hushchyn[44], D. Hutchcroft[61], M. Idzik[40], D. Ilin[44], P. Ilten[66], A. Iniukhin[44], A. Ishteev[44], K. Ivshin[44], H. Jage[17], S.J. Jaimes Elles[76,48,49], S. Jakobsen[49], E. Jans[38], B.K. Jashal[48], A. Jawahery[67], C. Jayaweera[54], V. Jevtic[19], Z. Jia[16], E. Jiang[67], X. Jiang[5,7], Y. Jiang[7], Y. J. Jiang[6], E. Jimenez Moya[9], N. Jindal[87], M. John[64], A. John Rubesh Rajan[23], D. Johnson[54], C.R. Jones[56], S. Joshi[42], B. Jost[49], J. Juan Castella[56], N. Jurik[49], I. Juszczak[41], D. Kaminaris[50], S. Kandybei[52], M. Kane[59], Y. Kang[4,d], C. Kar[11], M. Karacson[49], A. Kauniskangas[50], J.W. Kautz[66], M.K. Kazanecki[41], F. Keizer[49], M. Kenzie[56], T. Ketel[38], B. Khanji[69], A. Kharisova[44], S. Kholodenko[35,49], G. Khreich[14], T. Kirn[17], V.S. Kirsebom[31,p], O. Kitouni[65], S. Klaver[39], N. Kleijne[35,t], K. Klimaszewski[42], M.R. Kmiec[42], S. Koliiev[53], L. Kolk[19], A. Konoplyannikov[6], P. Kopciewicz[49], P. Koppenburg[38], A. Korchin[52], M. Korolev[44], I. Kostiuk[38], O. Kot[53], S. Kotriakhova, E. Kowalczyk[67], A. Kozachuk[44], P. Kravchenko[44], L. Kravchuk[44], M. Kreps[57], P. Krokovny[44], W. Krupa[69], W. Krzemien[42], O. Kshyvanskyi[53], S. Kubis[82], M. Kucharczyk[41], V. Kudryavtsev[44], E. Kulikova[44], A. Kupsc[84], V. Kushnir[52], B. Kutsenko[13], I. Kyryllin[52], D. Lacarrere[49], P. Laguarta Gonzalez[45], A. Lai[32], A. Lampis[32], D. Lancierini[62], C. Landesa Gomez[47], J.J. Lane[1], G. Lanfranchi[28], C. Langenbruch[22], J. Langer[19], O. Lantwin[44], T. Latham[57], F. Lazzari[35,u,49], C. Lazzeroni[54], R. Le Gac[13], H. Lee[61], R. Lefèvre[11], A. Leflat[44], S. Legotin[44], M. Lehuraux[57], E. Lemos Cid[49], O. Leroy[13], T. Lesiak[41], E. D. Lesser[49], B. Leverington[22], A. Li[4,d], C. Li[4], C. Li[13], H. Li[72], J. Li[8], K. Li[75], L. Li[63], M. Li[8], P. Li[7], P.-R. Li[73], Q. Li[5,7], T. Li[71], T. Li[72], Y. Li[8], Y. Li[5], Y. Li[4], Z. Lian[4,d], Q. Liang[8], X. Liang[69], S. Libralon[48], A. L. Lightbody[12], C. Lin[7], T. Lin[58], R. Lindner[49], H. Linton[62], R. Litvinov[32], D. Liu[8], F. L. Liu[1], G. Liu[72], K. Liu[73], S. Liu[5,7], W. Liu[8], Y. Liu[59], Y. Liu[73], Y. L. Liu[62], G. Loachamin Ordonez[70], A. Lobo Salvia[45], A. Loi[32], T. Long[56], J.H. Lopes[3], A. Lopez Huertas[45], C. Lopez Iribarnegaray[47], S. López Soliño[47], Q. Lu[15], C. Lucarelli[49], D. Lucchesi[33,r], M. Lucio Martinez[48], Y. Luo[6], A. Lupato[33,j], E. Luppi[26,m], K. Lynch[23], X.-R. Lyu[7], G. M. Ma[4,d], S. Maccolini[19], F. Machefert[14], F. Maciuc[43], B. Mack[69], I. Mackay[64], L. M. Mackey[69], L.R. Madhan Mohan[56], M. J. Madurai[54], D. Magdalinski[38], D. Maisuzenko[44], J.J. Malczewski[41], S. Malde[64], L. Malentacca[49], A. Malinin[44], T. Maltsev[44], G. Manca[32,l], G. Mancinelli[13], C. Mancuso[14], R. Manera Escalero[45], F. M. Manganella[37], D. Manuzzi[25], D. Marangotto[30,o], J.F. Marchand[10], R. Marchevski[50], U. Marconi[25], E. Mariani[16], S. Mariani[49], C. Marin Benito[45], J. Marks[22], A.M. Marshall[55], L. Martel[64], G. Martelli[34], G. Martellotti[36], L. Martinazzoli[49], M. Martinelli[31,p], D. Martinez Gomez[80], D. Martinez Santos[83], F. Martinez Vidal[48], A. Martorell i Granollers[46], A. Massafferri[2], R. Matev[49], A. Mathad[49], V. Matiunin[44], C. Matteuzzi[69], K.R. Mattioli[15], A. Mauri[62], E. Maurice[15], J. Mauricio[45], P. Mayencourt[50], J. Mazorra de Cos[48], M. Mazurek[42], M. McCann[62], T.H. McGrath[63], N.T. McHugh[60], A. McNab[63], R. McNulty[23], B. Meadows[66], G. Meier[19], D. Melnychuk[42], D. Mendoza Granada[16], F. M. Meng[4,d], M. Merk[38,81], A. Merli[50,30], L. Meyer Garcia[67], D. Miao[5,7], H. Miao[7], M. Mikhasenko[77], D.A. Milanes[76,z], A. Minotti[31,p], E. Minucci[28], T. Miralles[11], B. Mitreska[19], D.S. Mitzel[19], A. Modak[58], L. Moeser[19], R.D. Moise[17], E.

JHEP10(2025)169

F. Molina Cardenas[86], T. Mombächer[49], M. Monk[57,1], S. Monteil[11], A. Morcillo Gomez[47], G. Morello[28], M.J. Morello[35,t], M.P. Morgenthaler[22], J. Moron[40], W. Morren[38], A.B. Morris[49], A.G. Morris[13], R. Mountain[69], H. Mu[4,d], Z. M. Mu[6], E. Muhammad[57], F. Muheim[59], M. Mulder[80], K. Müller[51], F. Muñoz-Rojas[9], R. Murta[62], V. Mytrochenko[52], P. Naik[61], T. Nakada[50], R. Nandakumar[58], T. Nanut[49], I. Nasteva[3], M. Needham[59], E. Nekrasova[44], N. Neri[30,o], S. Neubert[18], N. Neufeld[49], P. Neustroev[44], J. Nicolini[49], D. Nicotra[81], E.M. Niel[15], N. Nikitin[44], Q. Niu[73], P. Nogarolli[3], P. Nogga[18], C. Normand[55], J. Novoa Fernandez[47], G. Nowak[66], C. Nunez[86], H. N. Nur[60], A. Oblakowska-Mucha[40], V. Obraztsov[44], T. Oeser[17], A. Okhotnikov[44], O. Okhrimenko[53], R. Oldeman[32,l], F. Oliva[59,49], E. Olivart Pino[45], M. Olocco[19], C.J.G. Onderwater[81], R.H. O'Neil[49], J.S. Ordonez Soto[11], D. Osthues[19], J.M. Otalora Goicochea[3], P. Owen[51], A. Oyanguren[48], O. Ozcelik[49], F. Paciolla[35,x], A. Padee[42], K.O. Padeken[18], B. Pagare[47], T. Pajero[49], A. Palano[24], M. Palutan[28], C. Pan[74], X. Pan[4,d], S. Panebianco[12], G. Panshin[5], L. Paolucci[57], A. Papanestis[58], M. Pappagallo[24,i], L.L. Pappalardo[26], C. Pappenheimer[66], C. Parkes[63], D. Parmar[77], B. Passalacqua[26,m], G. Passaleva[27], D. Passaro[35,t,49], A. Pastore[24], M. Patel[62], J. Patoc[64], C. Patrignani[25,k], A. Paul[69], C.J. Pawley[81], A. Pellegrino[38], J. Peng[5,7], X. Peng[73], M. Pepe Altarelli[28], S. Perazzini[25], D. Pereima[44], H. Pereira Da Costa[68], M. Pereira Martinez[47], A. Pereiro Castro[47], C. Perez[46], P. Perret[11], A. Perrevoort[80], A. Perro[49,13], M.J. Peters[66], K. Petridis[55], A. Petrolini[29,n], J. P. Pfaller[66], H. Pham[69], L. Pica[35,t], M. Piccini[34], L. Piccolo[32], B. Pietrzyk[10], G. Pietrzyk[14], R. N. Pilato[61], D. Pinci[36], F. Pisani[49], M. Pizzichemi[31,p,49], V. M. Placinta[43], M. Plo Casasus[47], T. Poeschl[49], F. Polci[16], M. Poli Lener[28], A. Poluektov[13], N. Polukhina[44], I. Polyakov[63], E. Polycarpo[3], S. Ponce[49], D. Popov[7,49], S. Poslavskii[44], K. Prasanth[59], C. Prouve[83], D. Provenzano[32,l,49], V. Pugatch[53], G. Punzi[35,u], S. Qasim[51], Q. Q. Qian[6], W. Qian[7], N. Qin[4,d], S. Qu[4,d], R. Quagliani[49], R.I. Rabadan Trejo[57], J.H. Rademacker[55], M. Rama[35], M. Ramírez García[86], V. Ramos De Oliveira[70], M. Ramos Pernas[57], M.S. Rangel[3], F. Ratnikov[44], G. Raven[39], M. Rebollo De Miguel[48], F. Redi[30,j], J. Reich[55], F. Reiss[20], Z. Ren[7], P.K. Resmi[64], M. Ribalda Galvez[45], R. Ribatti[50], G. Ricart[15,12], D. Riccardi[35,t], S. Ricciardi[58], K. Richardson[65], M. Richardson-Slipper[56], K. Rinnert[61], P. Robbe[14,49], G. Robertson[60], E. Rodrigues[61], A. Rodriguez Alvarez[45], E. Rodriguez Fernandez[47], J.A. Rodriguez Lopez[76], E. Rodriguez Rodriguez[49], J. Roensch[19], A. Rogachev[44], A. Rogovskiy[58], D.L. Rolf[19], P. Roloff[49], V. Romanovskiy[66], A. Romero Vidal[47], G. Romolini[26,49], F. Ronchetti[50], T. Rong[6], M. Rotondo[28], S. R. Roy[22], M.S. Rudolph[69], M. Ruiz Diaz[22], R.A. Ruiz Fernandez[47], J. Ruiz Vidal[81], J. J. Saavedra-Arias[9], J.J. Saborido Silva[47], S. E. R. Sacha Emile R.[49], R. Sadek[15], N. Sagidova[44], D. Sahoo[78], N. Sahoo[54], B. Saitta[32,l], M. Salomoni[31,49,p], I. Sanderswood[48], R. Santacesaria[36], C. Santamarina Rios[47], M. Santimaria[28], L. Santoro[2], E. Santovetti[37], A. Saputi, D. Saranin[44], A. Sarnatskiy[80], G. Sarpis[49], M. Sarpis[79], C. Satriano[36,v], M. Saur[73], D. Savrina[44], H. Sazak[17], F. Sborzacchi[49,28], A. Scarabotto[19], S. Schael[17], S. Scherl[61], M. Schiller[22], H. Schindler[49], M. Schmelling[21], B. Schmidt[49], S. Schmitt[17], H. Schmitz[18], O. Schneider[50], A. Schopper[62], N. Schulte[19], M.H. Schune[14], G. Schwering[17], B. Sciascia[28], A. Sciuccati[49], I. Segal[77], S. Sellam[47],

JHEP10(2025)169

A. Semennikov[44], T. Senger[51], M. Senghi Soares[39], A. Sergi[29,n], N. Serra[51], L. Sestini[27], A. Seuthe[19], B. Sevilla Sanjuan[46], Y. Shang[6], D.M. Shangase[86], M. Shapkin[44], R. S. Sharma[69], I. Shchemerov[44], L. Shchutska[50], T. Shears[61], L. Shekhtman[44], Z. Shen[38], S. Sheng[5,7], V. Shevchenko[44], B. Shi[7], Q. Shi[7], W. S. Shi[72], Y. Shimizu[14], E. Shmanin[25], R. Shorkin[44], J.D. Shupperd[69], R. Silva Coutinho[69], G. Simi[33,r], S. Simone[24,i], M. Singha[78], N. Skidmore[57], T. Skwarnicki[69], M.W. Slater[54], E. Smith[65], K. Smith[68], M. Smith[62], L. Soares Lavra[59], M.D. Sokoloff[66], F.J.P. Soler[60], A. Solomin[55], A. Solovev[44], N. S. Sommerfeld[18], R. Song[1], Y. Song[50], Y. Song[4,d], Y. S. Song[6], F.L. Souza De Almeida[69], B. Souza De Paula[3], K.M. Sowa[40], E. Spadaro Norella[29,n], E. Spedicato[25], J.G. Speer[19], P. Spradlin[60], V. Sriskaran[49], F. Stagni[49], M. Stahl[77], S. Stahl[49], S. Stanislaus[64], M. Stefaniak[87], E.N. Stein[49], O. Steinkamp[51], H. Stevens[19], D. Strekalina[44], Y. Su[7], F. Suljik[64], J. Sun[32], J. Sun[63], L. Sun[74], D. Sundfeld[2], W. Sutcliffe[51], K. Swientek[40], F. Swystun[56], A. Szabelski[42], T. Szumlak[40], Y. Tan[4,d], Y. Tang[74], Y. T. Tang[7], M.D. Tat[22], J. A. Teijeiro Jimenez[47], A. Terentev[44], F. Terzuoli[35,x], F. Teubert[49], E. Thomas[49], D.J.D. Thompson[54], A. R. Thomson-Strong[59], H. Tilquin[62], V. Tisserand[11], S. T'Jampens[10], M. Tobin[5], T. T. Todorov[20], L. Tomassetti[26,m], G. Tonani[30], X. Tong[6], T. Tork[30], D. Torres Machado[2], L. Toscano[19], D.Y. Tou[4,d], C. Trippl[46], G. Tuci[22], N. Tuning[38], L.H. Uecker[22], A. Ukleja[40], D.J. Unverzagt[22], A. Upadhyay[49], B. Urbach[59], A. Usachov[39], A. Ustyuzhanin[44], U. Uwer[22], V. Vagnoni[25], V. Valcarce Cadenas[47], G. Valenti[25], N. Valls Canudas[49], J. van Eldik[49], H. Van Hecke[68], E. van Herwijnen[62], C.B. Van Hulse[47,aa], R. Van Laak[50], M. van Veghel[38], G. Vasquez[51], R. Vazquez Gomez[45], P. Vazquez Regueiro[47], C. Vázquez Sierra[83], S. Vecchi[26], J.J. Velthuis[55], M. Veltri[27,y], A. Venkateswaran[50], M. Verdoglia[32], M. Vesterinen[57], W. Vetens[69], D. Vico Benet[64], P. Vidrier Villalba[45], M. Vieites Diaz[47], X. Vilasis-Cardona[46], E. Vilella Figueras[61], A. Villa[25], P. Vincent[16], B. Vivacqua[3], F.C. Volle[54], D. vom Bruch[13], N. Voropaev[44], K. Vos[81], C. Vrahas[59], J. Wagner[19], J. Walsh[35], E.J. Walton[1,57], G. Wan[6], A. Wang[7], B. Wang[5], C. Wang[22], G. Wang[8], H. Wang[73], J. Wang[6], J. Wang[5], J. Wang[4,d], J. Wang[74], M. Wang[49], N. W. Wang[7], R. Wang[55], X. Wang[8], X. Wang[72], X. W. Wang[62], Y. Wang[75], Y. Wang[6], Y. H. Wang[73], Z. Wang[14], Z. Wang[4,d], Z. Wang[30], J.A. Ward[57], M. Waterlaat[49], N.K. Watson[54], D. Websdale[62], Y. Wei[6], J. Wendel[83], B.D.C. Westhenry[55], C. White[56], M. Whitehead[60], E. Whiter[54], A.R. Wiederhold[63], D. Wiedner[19], M. A. Wiegertjes[38], C. Wild[64], G. Wilkinson[64,49], M.K. Wilkinson[66], M. Williams[65], M. J. Williams[49], M.R.J. Williams[59], R. Williams[56], S. Williams[55], Z. Williams[55], F.F. Wilson[58], M. Winn[12], W. Wislicki[42], M. Witek[41], L. Witola[19], T. Wolf[22], E. Wood[56], G. Wormser[14], S.A. Wotton[56], H. Wu[69], J. Wu[8], X. Wu[74], Y. Wu[6,56], Z. Wu[7], K. Wyllie[49], S. Xian[72], Z. Xiang[5], D. Xiao[8], Y. Xie[8], T. X. Xing[30], A. Xu[35,t], L. Xu[4,d], L. Xu[4,d], M. Xu[49], Z. Xu[49], Z. Xu[7], Z. Xu[5], K. Yang[62], X. Yang[6], Y. Yang[15], Z. Yang[6], V. Yeroshenko[14], H. Yeung[63], H. Yin[8], X. Yin[7], C. Y. Yu[6], J. Yu[71], X. Yuan[5], Y Yuan[5,7], E. Zaffaroni[50], M. Zavertyaev[21], M. Zdybal[41], F. Zenesini[25], C. Zeng[5,7], M. Zeng[4,d], C. Zhang[6], D. Zhang[8], J. Zhang[7], L. Zhang[4,d], R. Zhang[8], S. Zhang[71], S. Zhang[64], Y. Zhang[6], Y. Z. Zhang[4,d], Z. Zhang[4,d], Y. Zhao[22], A. Zhelezov[22], S. Z. Zheng[6], X. Z. Zheng[4,d], Y. Zheng[7],

JHEP10(2025)169

T. Zhou[6], X. Zhou[8], Y. Zhou[7], V. Zhovkovska[57], L. Z. Zhu[7], X. Zhu[4,d], X. Zhu[8], Y. Zhu[17], V. Zhukov[17], J. Zhuo[48], Q. Zou[5,7], D. Zuliani[33,r], G. Zunica[50]

[1] *School of Physics and Astronomy, Monash University, Melbourne, Australia*
[2] *Centro Brasileiro de Pesquisas Físicas (CBPF), Rio de Janeiro, Brazil*
[3] *Universidade Federal do Rio de Janeiro (UFRJ), Rio de Janeiro, Brazil*
[4] *Department of Engineering Physics, Tsinghua University, Beijing, China*
[5] *Institute Of High Energy Physics (IHEP), Beijing, China*
[6] *School of Physics State Key Laboratory of Nuclear Physics and Technology, Peking University, Beijing, China*
[7] *University of Chinese Academy of Sciences, Beijing, China*
[8] *Institute of Particle Physics, Central China Normal University, Wuhan, Hubei, China*
[9] *Consejo Nacional de Rectores (CONARE), San Jose, Costa Rica*
[10] *Université Savoie Mont Blanc, CNRS, IN2P3-LAPP, Annecy, France*
[11] *Université Clermont Auvergne, CNRS/IN2P3, LPC, Clermont-Ferrand, France*
[12] *Université Paris-Saclay, Centre d'Etudes de Saclay (CEA), IRFU, Saclay, France, Gif-Sur-Yvette, France*
[13] *Aix Marseille Univ, CNRS/IN2P3, CPPM, Marseille, France*
[14] *Université Paris-Saclay, CNRS/IN2P3, IJCLab, Orsay, France*
[15] *Laboratoire Leprince-Ringuet, CNRS/IN2P3, Ecole Polytechnique, Institut Polytechnique de Paris, Palaiseau, France*
[16] *LPNHE, Sorbonne Université, Paris Diderot Sorbonne Paris Cité, CNRS/IN2P3, Paris, France*
[17] *I. Physikalisches Institut, RWTH Aachen University, Aachen, Germany*
[18] *Universität Bonn — Helmholtz-Institut für Strahlen und Kernphysik, Bonn, Germany*
[19] *Fakultät Physik, Technische Universität Dortmund, Dortmund, Germany*
[20] *Physikalisches Institut, Albert-Ludwigs-Universität Freiburg, Freiburg, Germany*
[21] *Max-Planck-Institut für Kernphysik (MPIK), Heidelberg, Germany*
[22] *Physikalisches Institut, Ruprecht-Karls-Universität Heidelberg, Heidelberg, Germany*
[23] *School of Physics, University College Dublin, Dublin, Ireland*
[24] *INFN Sezione di Bari, Bari, Italy*
[25] *INFN Sezione di Bologna, Bologna, Italy*
[26] *INFN Sezione di Ferrara, Ferrara, Italy*
[27] *INFN Sezione di Firenze, Firenze, Italy*
[28] *INFN Laboratori Nazionali di Frascati, Frascati, Italy*
[29] *INFN Sezione di Genova, Genova, Italy*
[30] *INFN Sezione di Milano, Milano, Italy*
[31] *INFN Sezione di Milano-Bicocca, Milano, Italy*
[32] *INFN Sezione di Cagliari, Monserrato, Italy*
[33] *INFN Sezione di Padova, Padova, Italy*
[34] *INFN Sezione di Perugia, Perugia, Italy*
[35] *INFN Sezione di Pisa, Pisa, Italy*
[36] *INFN Sezione di Roma La Sapienza, Roma, Italy*
[37] *INFN Sezione di Roma Tor Vergata, Roma, Italy*
[38] *Nikhef National Institute for Subatomic Physics, Amsterdam, Netherlands*
[39] *Nikhef National Institute for Subatomic Physics and VU University Amsterdam, Amsterdam, Netherlands*
[40] *AGH — University of Krakow, Faculty of Physics and Applied Computer Science, Kraków, Poland*
[41] *Henryk Niewodniczanski Institute of Nuclear Physics Polish Academy of Sciences, Kraków, Poland*
[42] *National Center for Nuclear Research (NCBJ), Warsaw, Poland*
[43] *Horia Hulubei National Institute of Physics and Nuclear Engineering, Bucharest-Magurele, Romania*
[44] *Authors affiliated with an institute formerly covered by a cooperation agreement with CERN.*
[45] *ICCUB, Universitat de Barcelona, Barcelona, Spain*
[46] *La Salle, Universitat Ramon Llull, Barcelona, Spain*
[47] *Instituto Galego de Física de Altas Enerxías (IGFAE), Universidade de Santiago de Compostela, Santiago de Compostela, Spain*

JHEP10(2025)169

[48] Instituto de Fisica Corpuscular, Centro Mixto Universidad de Valencia — CSIC, Valencia, Spain
[49] European Organization for Nuclear Research (CERN), Geneva, Switzerland
[50] Institute of Physics, Ecole Polytechnique Fédérale de Lausanne (EPFL), Lausanne, Switzerland
[51] Physik-Institut, Universität Zürich, Zürich, Switzerland
[52] NSC Kharkiv Institute of Physics and Technology (NSC KIPT), Kharkiv, Ukraine
[53] Institute for Nuclear Research of the National Academy of Sciences (KINR), Kyiv, Ukraine
[54] School of Physics and Astronomy, University of Birmingham, Birmingham, United Kingdom
[55] H.H. Wills Physics Laboratory, University of Bristol, Bristol, United Kingdom
[56] Cavendish Laboratory, University of Cambridge, Cambridge, United Kingdom
[57] Department of Physics, University of Warwick, Coventry, United Kingdom
[58] STFC Rutherford Appleton Laboratory, Didcot, United Kingdom
[59] School of Physics and Astronomy, University of Edinburgh, Edinburgh, United Kingdom
[60] School of Physics and Astronomy, University of Glasgow, Glasgow, United Kingdom
[61] Oliver Lodge Laboratory, University of Liverpool, Liverpool, United Kingdom
[62] Imperial College London, London, United Kingdom
[63] Department of Physics and Astronomy, University of Manchester, Manchester, United Kingdom
[64] Department of Physics, University of Oxford, Oxford, United Kingdom
[65] Massachusetts Institute of Technology, Cambridge, MA, United States
[66] University of Cincinnati, Cincinnati, OH, United States
[67] University of Maryland, College Park, MD, United States
[68] Los Alamos National Laboratory (LANL), Los Alamos, NM, United States
[69] Syracuse University, Syracuse, NY, United States
[70] Pontifícia Universidade Católica do Rio de Janeiro (PUC-Rio), Rio de Janeiro, Brazil, associated to [3]
[71] School of Physics and Electronics, Hunan University, Changsha City, China, associated to [8]
[72] Guangdong Provincial Key Laboratory of Nuclear Science, Guangdong-Hong Kong Joint Laboratory of Quantum Matter, Institute of Quantum Matter, South China Normal University, Guangzhou, China, associated to [4]
[73] Lanzhou University, Lanzhou, China, associated to [5]
[74] School of Physics and Technology, Wuhan University, Wuhan, China, associated to [4]
[75] Henan Normal University, Xinxiang, China, associated to [8]
[76] Departamento de Fisica, Universidad Nacional de Colombia, Bogota, Colombia, associated to [16]
[77] Ruhr Universitaet Bochum, Fakultaet f. Physik und Astronomie, Bochum, Germany, associated to [19]
[78] Eotvos Lorand University, Budapest, Hungary, associated to [49]
[79] Faculty of Physics, Vilnius University, Vilnius, Lithuania, associated to [20]
[80] Van Swinderen Institute, University of Groningen, Groningen, Netherlands, associated to [38]
[81] Universiteit Maastricht, Maastricht, Netherlands, associated to [38]
[82] Tadeusz Kosciuszko Cracow University of Technology, Cracow, Poland, associated to [41]
[83] Universidade da Coruña, A Coruña, Spain, associated to [46]
[84] Department of Physics and Astronomy, Uppsala University, Uppsala, Sweden, associated to [60]
[85] Taras Schevchenko University of Kyiv, Faculty of Physics, Kyiv, Ukraine, associated to [14]
[86] University of Michigan, Ann Arbor, MI, United States, associated to [69]
[87] Ohio State University, Columbus, United States, associated to [68]

[a] Universidade Estadual de Campinas (UNICAMP), Campinas, Brazil
[b] Centro Federal de Educacão Tecnológica Celso Suckow da Fonseca, Rio De Janeiro, Brazil
[c] Department of Physics and Astronomy, University of Victoria, Victoria, Canada
[d] Center for High Energy Physics, Tsinghua University, Beijing, China
[e] Hangzhou Institute for Advanced Study, UCAS, Hangzhou, China
[f] LIP6, Sorbonne Université, Paris, France
[g] Lamarr Institute for Machine Learning and Artificial Intelligence, Dortmund, Germany
[h] Universidad Nacional Autónoma de Honduras, Tegucigalpa, Honduras
[i] Università di Bari, Bari, Italy
[j] Università di Bergamo, Bergamo, Italy
[k] Università di Bologna, Bologna, Italy

JHEP10(2025)169

[l] Università di Cagliari, Cagliari, Italy
[m] Università di Ferrara, Ferrara, Italy
[n] Università di Genova, Genova, Italy
[o] Università degli Studi di Milano, Milano, Italy
[p] Università degli Studi di Milano-Bicocca, Milano, Italy
[q] Università di Modena e Reggio Emilia, Modena, Italy
[r] Università di Padova, Padova, Italy
[s] Università di Perugia, Perugia, Italy
[t] Scuola Normale Superiore, Pisa, Italy
[u] Università di Pisa, Pisa, Italy
[v] Università della Basilicata, Potenza, Italy
[w] Università di Roma Tor Vergata, Roma, Italy
[x] Università di Siena, Siena, Italy
[y] Università di Urbino, Urbino, Italy
[z] Universidad de Ingeniería y Tecnología (UTEC), Lima, Peru
[aa] Universidad de Alcalá, Alcalá de Henares, Spain
[†] Deceased

JHEP10(2025)169